A novel transcript of LncRNA ELDR promotes chondrocyte senescence and osteoarthritis progression by tuning chromosomal dynamics

Jun Lu (junlusuper@outlook.com)
The Center of Joint and Sports Medicine, Orthopedics Department, Zhongda Hospital, Southeast University

Ming liang ji
Zhongda Hospital, School of Medicine, Southeast University

Zhuang Li
The Center of Joint and Sports Medicine, Orthopedics Department, Zhongda Hospital, Southeast University

Qing Chang
The Center of Joint and Sports Medicine, Orthopedics Department, Zhongda Hospital, Southeast University

Rui Geng
The Center of Joint and Sports Medicine, Orthopedics Department, Zhongda Hospital, Southeast University

Zhi wen Zhou
The Center of Joint and Sports Medicine, Orthopedics Department, Zhongda Hospital, Southeast University

Yu cheng Lin
Southeast University

Article

Keywords: aging, chondrocyte senescence, osteoarthritis, non-coding RNA, epigenetics

Posted Date: June 10th, 2022

DOI: https://doi.org/10.21203/rs.3.rs-1645805/v1

A novel transcript of LncRNA ELDR promotes chondrocyte senescence and osteoarthritis progression by tuning chromosomal dynamics

Brief summary: LncRNA ELDR in chondrocyte senescence and osteoarthritis

Keywords: aging; chondrocyte senescence; osteoarthritis; non-coding RNA; epigenetics

Abstract

Epigenetic reprogramming plays a critical role in chondrocyte senescence during osteoarthritis (OA) pathology, but the underlying molecular mechanisms remain to be elucidated. Here using large-scale patient data sets and genetically engineered (Col2a1-CreER^{T2};Eldr$^{flox/flox}$ and Col2a1-CreER^{T2};ROSA26-LSL-Eldr$^{+/+}$ KI) mouse models, we show that a novel transcript of long noncoding RNA ELDR is essential for the development of chondrocyte senescence. ELDR is highly expressed in chondrocytes and cartilage tissues of OA. Mechanistically, exon 4 of ELDR physically mediates a complex consisting of hnRNPL and KAT6A to regulate histone modifications of the promoter region of the IHH gene, thereby activating hedgehog signaling and promoting chondrocyte senescence. Therapeutically, GapmeR-mediated silencing of ELDR in OA model substantially attenuates chondrocyte senescence and cartilage degradation. Clinically, ELDR knockdown in cartilage explants from OA patients decreased the expression of senescence markers and catabolic mediators. Taken together, these findings uncover a previously uncharacterized lncRNA-dependent epigenetic driver in chondrocyte senescence, highlighting that ELDR could be a promising therapeutic avenue for OA.

Introduction

Aging and trauma are crucial risk factors for the development of osteoarthritis (OA)[1-4], a highly prevalent and severely debilitating whole-joint disorder predominantly characterized by destruction of articular cartilage causing pain and functional disability[5-8]. Although the relationship between aging and OA is not fully understood, accumulating evidence suggests that aging-associated changes in articular tissues contribute to OA development[3,4,9]. From studies of surgically-induced OA in young animals, osteoarthritic phenotypes in the joint can develop without a substantial contribution of aging, implying that aging and OA are inter-related but not inter-dependent[3,10]. Hence, a deeper understanding of how aging and trauma drive OA will undoubtedly enable the identification of a variety of potential therapeutic targets aiming to slow or stop the progression of this chronic and disabling condition, which would have a major impact on public health.

In a physiological setting, the chondrocyte, the unique resident cell type in articular cartilage, maintains cartilage homeostasis via a delicate balance between anabolism and catabolism[11,12] Under various pathological stimuli, chondrocytes undergo phenotypic shift, developing features of a senescent phenotype [13,14]. Mounting evidence shows that chondrocyte senescence is potentially a common molecular mechanism that drives or promotes both age-associated and post-traumatic OA, with senescent chondrocytes exhibiting a variety of the senescence-associated secretory phenotype (SASP)[15,16], which ultimately results in breakdown of the articular cartilage. Several senescent cells (SnCs) markers, including SA-β-gal, expression levels of $p16^{INK4A}$ and p21 etc, are found in osteoarthritic cartilage[2]. More intriguingly, clearance of SnCs through a transgenic system or pharmaceutical intervention (local intra- articular injection of UBX0101) decreased expression of senescent and inflammatory markers while also increased expression of cartilage tissue extracellular matrix proteins, implicating that targeting SnCs might be an attractive therapeutic modality for treatment of OA [2,17,18]. However, the regulatory mechanisms underlying the senescent phenotypes of chondrocytes is not well characterized, and how these phenotypes can be controlled in OA cartilage remains poorly understood.

Long non-coding RNAs (lncRNAs), which fulfills regulatory roles at almost every stage of gene expression from targeting epigenetic modifications in the nucleus to modulating mRNA stability and translation in the cytoplasm, can bind DNA, RNA, or proteins to regulate cellular

senescence[4,19-21]. For instance, silencing of GUARDIN, a p53-responsive lncRNA, leads to senescence, whereas the lncRNA PANDA recruits PcG complexes, suppressing senescence-promoting genes[22]. Similarly, silencing lncRNA-OIS1 diminishes the senescent-associated induction of a nearby gene (Dipeptidyl Peptidase 4, DPP4) with established role in tumor suppression[23]. Also, lncRNA UCA1 and CAPERα/TBX3 constitute a coordinated, reinforcing mechanism to regulate both CDKN2A-p16^{INK} transcription and mRNA stability, inducing senescence[24]. LncRNAs have important functions in both development and diseases of the joints[25-27]; however, precise mechanisms of lncRNAs in chondrocyte senescence and cartilage degradation of OA have not yet been thoroughly investigated.

Here, we identified a novel transcript of EGFR long non-coding downstream RNA (ELDR), which was markedly upregulated in OA and significantly associated with cartilage degradation. The biological roles of ELDR in chondrocyte senescence and OA development were genetically assessed in several in vitro and in vivo models.

Results

ELDR is a cartilage senescence-associated lncRNA

To investigate lncRNA transcriptome changes during OA, the Arraystar human lncRNA+mRNA Array V4.0 (8 x 60K format) was employed to profile the lncRNA expression in OA (n=3) and normal (n=3) cartilage tissues (Figure 1A and Figure S1A). A set of stringent criteria were used to filter LncRNAs: (1) fold change > 10 or < 0.1 and a p value < 0.05, (2) >200 nucleotides (nt) in length, (3) “Gold” for LncRNA level, (3) no overlap with protein-coding regions or pseudogenes[28], and (4) low predicted coding probability[29], 38 dysregulated lncRNAs (23 upregulation and 15 downregulation) were selected for further investigation (Figure 1B and C). We then tested these 38 LncRNAs using an independent cohort of 21 controls and 42 OA patients. SHANK2-AS2, ELDR, LINC01521, LINC01159 and RP11-802E16.3 were observed to be significantly dysregulated (Table S1). These five LncRNAs were further evaluated by RT-qPCR using additional independent cohort comprising of 32 controls and 63 OA patients. Of the five LncRNAs, LINC01521 and ELDR were found to be significantly upregulated in OA patients compared with controls (Table S1). Finally, we focused on the most upregulated ELDR for further investigation. Compared to controls, severe cartilage degradation and synovitis were observed in

OA patients (Figure 1D). RT-qPCR results demonstrated that ELDR expression level was significantly overexpressed in 105 cartilage tissues from OA patients compared with 53 controls and in chondrocytes (Figure 1E). ELDR is located at human chromosome 7p11.2, harbouring four exons, and is highly conserved in different species (Figure S1B and C). Of interest, ELDR was specifically elevated in human cartilage (Figure S1D). However, the shorter form of ELDR was not detected in human cartilage (Figure S1E). We performed 5' and 3' rapid amplification of complementary DNA ends, and found that a novel transcript of ELDR contains 2724 nucleotides with a poly(A) tail, which is transcribed from exons 1, 3 and 4 through analyzing UCSC, Ensembl and LNCipedia database (Figure 1F and Figure S1F). In addition, the full length (2724nt) was further validated by northern blot (Figure S1G). The non-coding nature of ELDR was confirmed by Coding Potential Calculator (CPC) and Coding-Potential Assessment Tool (CPAT) analysis (Figure 1G).

Dysregulated mRNAs profile was also analyzed in OA (Figure S1H). All these genes were subjected to gene ontology (GO) analysis. Upregulated gene GO terms with the most significant p values for biological processes, molecular function, and cellular component were related to replicative senescence (GO:0090399), tumor necrosis factor-activated receptor activity (GO:0005031) and interleukin-6 receptor complex (GO:0005896) (Figure S1H), indicating the important role of celluar senescence in human OA. Importantly, high levels of senescence markers were found. The expressions of $p16^{INK4a}$ and SASP (TNF-α, IL-1β and IL-6) were further characterized in OA and the controls. $p16^{INK4a}$, TNF-α, IL-1β and IL-6 were markedly elevated in OA compared to controls (Figure 1H and Figure S1I), which was further confirmed by our analysis of single-cell RNA sequencing (scRNA-seq) data from GEO database[13] and immunofluorescence staining (Figure 1I and Figure 1J). We quantified telomere length in chondrocytes isolated from OA cartilage tissues and controls using real-time PCR and FISH. Osteoarthritic chondrocytes had shorter telomeres and fewer telomere foci than controls (Figure 1K and L). Increased senescence-associated-galactosidase (SA-β-Gal) positivity was also observed (Figure 1M). Given the key role of LncRNAs in cellular senescence[4], we explored a possible association between ELDR and chondrocyte senescence. ELDR expression level correlated with the modified Mankin scale, $p16^{INK4a}$, TNF-α, IL-1β and IL-6 levels (Figure S1J). More importantly, gain-of-function and loss-of-function experiments showed that upregulation or

downregulation of ELDR remarkably affected $p16^{INK4a}$ and SASP expressions (Figure 1N and Figure S1K). These data imply that the novel transcript of ELDR is critical for osteoarthritic phenotype.

The critical role of Eldr in embryonic chondrocyte senescence

To investigate the involvement of Eldr gene in chondrocyte senescence during embryo, Eldr knockout (KO) and Eldr ROSA26 knockin (KI) mice were constructed using CRISPR/Cas9 based EGE system (Figure 2A, B, S2A and B). We then crossed Col2a1-$CreER^{T2}$ mice with $Eldr^{flox/flox}$ and Eldr knock-in (KI) ($Eldr^{ROSA26}$) mice to generate chondrocyte - specific Eldr KO and KI mice. Pregnant mice with embryos at E10.5 were injected with tamoxifen (TM). Intriguingly, we found that the expression levels of $p16^{INK4a}$, p21, p53 and SASPs (IL-6, TNF-α and MMP3) were upregulated at E14.5 and E18.5 of Eldr cKI mice compared with Eldr cKO mice (Figure 2C and D). Further, high levels of $p16^{INK4a}$ and p21 in Eldr cKI mice were confirmed by immunofluorescence staining (Figure 2E and F). At E14.5 and E18.5, chondrocytes in proliferative zone of Eldr cKO mice had relatively high proliferation, compared with Eldr cKI mice (Figure 2G and H). Whether these senescent chondrocytes that lost senescent hallmarks during embryogenesis can re-enter cell cycle or survive in the cartilage after birth warrants further investigation in future. Taken together, these data reveal that Eldr plays a key role in maintaining chondrocyte metabolism and determining the fate of senescent chondrocytes during embryogenesis.

Eldr regulates aging and injury-induced chondrocyte senescence during OA

Chondrocyte senescence is considered a crucial cellular event contributing to extracellular matrix remodeling, which promotes age-related and post-traumatic OA progression[2,3,15,30-32]. In order to investigate the role of Eldr in chondrocyte senescence in vivo, Eldr knockout (KO) and Eldr ROSA26 knockin (KI) mice were constructed using CRISPR/Cas9 based EGE system. We then crossed Col2a1-$CreER^{T2}$ mice with $Eldr^{flox/flox}$ and Eldr knock-in (KI) ($Eldr^{ROSA26}$) mice to generate chondrocyte-specific Eldr KO and KI mice. We observed spontaneously developed OA in Eldr cKO and Eldr cKI mice with aging (Figure S3A). $Eldr^{flox/flox}$, Eldr cKO, $Eldr^{ROSA26}$ and Eldr cKI (8 weeks old) mice were injected intraperitoneally with tamoxifen (100 μg/g body weight) daily for 5 days. Of note, remarkable senescence phenotypes such as induction of $p16^{INK4a}$, up-regulation of IL-6, MMP3 and increased SA-β-Gal positivity were detected at postnatal month

6 (P6M) (Figure 3A), P12M (Figure 3B) and P18M (Figure 3C) in Eldr cKI mice compared with Eldr cKO, $Eldr^{flox/flox}$ and $Eldr^{ROSA26}$ mice. Furthermore, histological analysis for P6M Eldr cKI mice showed some loss of proteoglycans, roughening of the articular cartilage, and some loss of articular chondrocyte cellularity compared to Eldr cKO mice (Figure 3D). By P12M, greater loss of proteoglycans, the loss of cellularity and destruction in some regions of the articular cartilage were noted in Eldr cKI mice (Figure 3D). By P18M, this phenotype became more profound, and Eldr cKI mice showed significant and severe destruction of the articular cartilage (Figure 3D). These results were confirmed by the significant increase in the OARSI and synovitis scores (Figure 3D). Subsequently, we induced post-traumatic OA by surgical destabilisation of medial meniscus (DMM) in wild type (WT), Eldr cKO and Eldr cKI mice. Compared to WT and Eldr cKO mice, senescence markers was significantly increased in Eldr cKI mice (Figure 3E). Of interest, Eldr cKO mice exhibited markedly reduced cartilage degradation and significantly lower OARSI grades at 8 weeks after DMM surgery (Figure 3F). The Ki67, Col2a1 and MMP13 levels were analyzed by immunohistochemistry (Figure 3G). Moreover, significantly decreased chondrocyte apoptosis Eldr cKO mice was observed (Figure 3H, Figure S3B and Figure S3C). By EdU incorporation assay, we also found a remarkable increase in the number of EdU+ chondrocytes in Eldr cKO cartilage compared with $Eldr^{flox/flox}$ and $Eldr^{ROSA26}$ mice undergoing sham surgery and Eldr cKI mice undergoing DMM surgery (Figure 3I). During OA development, Eldr was highly expressed (Figure S3D). These data demonstrate that ablation of Eldr inhibits chondrocyte senescence and SASP in vivo, implying that common mechanisms are at play between aging- and injury-induced SnCs.

ELDR forms a RNA-DNA triplex with the IHH gene promoter

A detailed understanding of how chondrocytes enter the senescent state might enable the development of therapies designed to prevent such a phenotypic switch during OA. We then investigated ELDR-mediated transcriptional targets that could account for chondrocyte senescence during the pathogenesis of OA. RNA-seq analysis was performed in ELDR cKO and cKI chondrocytes from mice. In ELDR cKO chondrocytes, the enriched genes were associated with regulation of cartilage development (GO:0061035), collagen-containing extracellular matrix (GO:0062023) and extracellular matrix constituent, lubricant activity (GO:0030197) (Figure 4A). In ELDR cKI chondrocytes, the enriched genes were related to cellular senescence (GO:0090398),

DNA repair complex (GO:1990391) and chemokine activity (GO:0008009) (Figure 4B). These results suggest that ELDR is closely involved in chondrocyte homeostasis. Among these significantly differentially expressed genes regulated by ELDR, 5 genes that have previously been reported to be associated with OA were found to be significantly dysregulated[12,13,33-35]. RT-qPCR was then performed to measure these genes. The results showed that HPIP, ITGBL1 and IHH were downregulated in ELDR cKO chondrocytes and upregulated in ELDR cKI chondrocytes (Figure 4C). Furthermore, KEGG pathway analysis demonstrated that Hedgehog signaling pathway was markedly dysregulated (Figure 4D). More importantly, expression levels of IHH, Ptch1, Gli, $p16^{INK4a}$, TNF-α, IL-1β, IL-6, MMP13 and ADAMTS5 were significantly increased in ELDR cKI chondrocytes, whereas expression levels of HMGB1, Col II and Aggrecan were downregulated (Figure 4E and Figure S4A). The opposite results were observed in ELDR cKO chondrocytes (Figure 4E and Figure S4A). Rescue experiments were further performed to validate the relationship between ELDR and IHH signaling pathway (Figure S4B). These results provide direct evidence that IHH plays a vital role in ELDR-induced chondrocyte senescence.

Notably, we observed that ELDR depletion did not affect the expression of its nearby genes (Figure S4C), thus suggesting that ELDR regulates IHH in trans. To further clarify the mechanisms underlying ELDR-induced IHH expression, we performed FISH and subcellular fractionation assays and demonstrated that ELDR was predominantly localized to the nucleus, which implies that ELDR exerts its biological function in the nucleus (Figure 4F and G). Then, we generated a series of IHH-luc promoter constructs, located from -2000bp upstream to +200bp downstream of the transcriptional start site to explore whether ELDR transcriptionally upregulated IHH. As shown in Figure 4H, the promoter luciferase assay showed that the -550 to +200bp region of IHH promoter led to an obvious increase of transcriptional activity. Moreover, chromatin isolation by RNA purification (ChIRP) assays showed that ELDR interacted physiologically with the (-476 to -453bp) region in the IHH promoter in chondrocytes (Figure 4I and J). To further identify the direct binding sites between ELDR and IHH promoter, five potential pairs of triplex-forming oligonucleotides (TFOs) and their corresponding triplex target sites (TTS) in the ELDR and IHH promoter were obtained from LongTarget. Each binding motif was subjected to fluorescence resonance energy transfer (FRET) analysis and circular dichroism (CD) spectroscopy. FRET demonstrated an obvious increase in fluorescence intensity at 570-580nm and a decrease at

520nm in the ELDR (1138-1152nt)/IHH-TTS1 (-476 to -453bp) group compared with that of the control ssRNA/IHH TTS group, which was in accordance with the FENDRR/PITX2 positive control group (Figure 4K and Figure S4C), suggesting energy transfer from the fluorescein donor to the rhodamine acceptor and promoting the formation of triple helices. CD displayed that the ELDR (1138-1152nt)/IHH-TTS1 (-476 to -453bp) group had a strong positive peak at 270-280nm and a deep negative peak at 210nm (Figure 4L). This was in accordance with the FENDRR/PITX2-positive control group (Figure S4D), indicating that ELDR directly formed triplexes with the IHH promoter sequence in vitro. ELDR that was mutated at 1138-1152nt failed to induce IHH expression (Figure 4M). Moreover, ELDR enhanced the luciferase intensity of the IHH promoter, while no obvious change was observed in the mutated IHH promoter (Figure 4N and Figure S4E), indicating that the sequence between 1138-1152nt in ELDR and -476 to -453bp in the IHH promoter are of great significance for ELDR-induced IHH activation. These data suggest that ELDR regulates IHH transcription through direct triplex formation with the promoter sequence.

To determine the upstream factor regulating ELDR during chondrocyte senescence, we analyzed the 5' and intron sequences of ELDR, EGFR long non-coding downstream RNA, and found that there are three canonical EGFR binding sites (E-Boxes) in this region (Figure S4F), raising the possibility that ELDR is a direct target of EGFR. Knocking down or overexpressing EGFR led to downregulating or upregulating ELDR transcription, respectively (Figure 4O). Luciferase activity assay showed that EGFR could directly promote ELDR transcription. Unlike enhancers, the activity of a promoter is usually orientation dependent (Figure 4P). Furthermore, ChIP analysis demonstrated that EGFR was found to strongly bind to 5' E-Box and 3' E-Box tandem in the ELDR promoter (Figure 4Q). Together, these findings demonstrate that ELDR is a direct EGFR target.

ELDR recruits hnRNPL and KAT6A to IHH promoter and promotes its H3K4me3 and H3K9ac

LncRNAs can bind to transcriptional factors, histone regulators or other cellular factors to modulate downstream gene expression, serving as scaffolds for the histone modification complex[36,37]. We subsequently performed an RNA pull down assay using in vitro transcribed biotinylated ELDR and an antisense control to identify ELDR-interacting proteins in chondrocytes.

Two bands at about 64 and 225kDa, respectively, were specifically enriched in the ELDR pull down proteins (Figure 5A). Using mass spectrometry, hnRNPL and KAT6A were identified as the most abundant ELDR-interacting proteins (Figure 5B and Figure S5A). Western Blot analysis further indicated that ELDR bounded specifically to hnRNPL and KAT6A (Figure 5C and Figure S5B). RNA in situ hybridization-proximity ligation assay (rISH-PLA) showed the proximity of ELDR to endogenous hnRNPL or KAT6A in the nucleus of cultured human primary chondrocyte and SW1353 (Figure 5D and Figure S5C). RIP assays demonstrated that ELDR directly interacted with hnRNPL and KAT6A (Figure 5E). Serial deletion analysis demonstrated that exon 4 of the ELDR transcript (1640-1680nt) was necessary and sufficient to bind hnRNPL and KAT6A (Figure 5F), which was further confirmed by RNA pull down, western blotting and an RNA electrical mobility shift assay (EMSA) (Figure 5G). RNA-binding protein (RBP) binding site for hnRNPL and KAT6A was located in the 1640-1680nt region of exon 4 of the ELDR and formed a stem-loop structure (Figure 5H). The direct interaction of exon 4 of the WT ELDR transcript with hnRNPL and KAT6A was further confirmed by molecular dynamics trajectory (Figure 5I and Figure S5D). RIP performed after site-directed mutagenesis of this region revealed that it was critical to ELDR interaction with hnRNPL and KAT6A (Figure 5J).

hnRNPL and KAT6A epigenetically regulates target gene expression by association with H3K4me3 and H3K9ac[38]. To further confirm that ELDR activated IHH expression by interacting with hnRNPL and KAT6A, ChIP analysis was performed and showed that ELDR overexpression dramatically enhanced hnRNPL and KAT6A occupancy at IHH promoter and increased H3K4me3 and H3K9ac of the promoters of IHH (Figure 5K and Figure S5E), whereas mutated ELDR drastically decreased hnRNPL and KAT6A occupancy and H3K4me3 and H3K9ac of the IHH promoter (Figure 5K and Figure S5E). Moreover, silencing hnRNPL or KAT6A attenuated the increased effect of ELDR on the transcriptional activation of IHH, whereas hnRNPL or KAT6A overexpression partly restored the expression of IHH after ELDR silencing (Figure 5L). Taken together, these data imply that ELDR regulates IHH expression through hnRNPL and KAT6A mediated H3K4me3 and H3K9ac, respectively.

ELDR/hnRNPL/KAT6A complex facilitates the binding between NRF1 and IHH promoter sequence

Dynamic changes at specific chromosomal loci have been demonstrated to expose protein-binding

sites, thereby allowing the recruitment of trans-factors and resulting in the alteration of gene transcription[39]. To address whether ELDR modulates hnRNPL and KAT6A genomic binding genome-wide, we performed ChIP-seq for hnRNPL and KAT6A in chondrocytes. The ChIP-seq data (hnRNPL and KAT6A) showed 4580 and 5936 called peaks, respectively, in chondrocytes transfected with GapmeR-scrambled control. GapmeR-ELDR caused reduced hnRNPL and KAT6A occupancies in these two histone modulator binding DNA regions (Figure 6A and B). A substantial subset of genes that exhibit decreased binding by the hnRNPL/KAT6A complex were dysregulated after knockdown of ELDR (Figure 6C). Integrative GSEA of the RNA-seq and hnRNPL/KAT6A ChIP-seq data revealed significant enrichment for genes that were downregulated when ELDR was silenced (Figure 6D). Furthermore, ATAC-seq data from Cristrome Data Browser was comprehensively analyzed. We found that the chromosomal region chr2q35 (IHH) had an open status in OA and chondrocytes, and NRF1, an important transcripition factor in OA pathogenesis[40,41], was recruited onto the IHH promoter (Figure 6E). With DNA pull-down and mass spectrometry analysis, one binding band to IHH was identified to be NRF1 (Figure 6F, Figure 6G and Figure S6A). Furthermore, the NRF1 expression level was determined in chondrocytes and cartilage tissues from human and mice OA (Figure 6H and I). Since histone modification is an important indicator in dynamic chromatin tuning, we then detected the changes of histone methylation and acetylation in IHH promoter using ChIP-seq data (GSM670034, GSM670004, GSM669990, GSM670030 and GSM669917). The data showed high levels of H3K4me3, H3K9ac and H3K4me1 in its promoter (Figure 6J), which was further confirmed by the analysis in human OA and control chondrocytes (Figure 6J).

To further study the formation of the ELDR/epigenetic modulator complex/transcription factor, we performed coimmu-noprecipitation (co-IP) using hemagglutinin (HA)-tagged beads and found that NRF1 did not directly interact with hnRNPL or KAT6A (Figure 6K), whereas the results of the RNA pull-down assay showed that ELDR could interact with both hnRNPL and KAT6A (Figure 5A and B). The ChIP analysis revealed that NRF1 could interact with IHH promoter and that this interaction was dependent on high expression of ELDR (Figure 6L). However, the interaction between NRF1 and IHH promoter was not detected in chondrocytes overexpressing ELDR while hnRNPL and KAT6A knockdown (Figure 6M). In contrast, the binding between NRF1 and IHH promoter was not observed in ELDR knockdown, although overexpressing

hnRNPL and KAT6A (Figure 6M). Theses data indicate that open chromatin status in IHH promoter induced by ELDR/hnRNPL/KAT6A complex provides a unique opportunity for NRF1 binding onto the IHH promoter, initiating IHH signaling expression and chondrocyte senescence (Figure 6N). Therefore, our findings form the basis for the exploration of chromatin dynamics biology and provide potential targets for the diagnosis and treatment of OA.

Therapeutic depletion of ELDR inhibits chondrocyte senescence and OA progression

Eliminating senescent cells and attenuating the SASP have emerged as attractive therapeutic strategies[32]; however, translation of these findings into relevant human applications is currently limited by our fragmentary understanding of both the basic molecular cell biology of in vivo senescent cells. We therefore sought to investigate the therapeutic role of Eldr in OA and to elucidate the underlying molecular mechanisms involved, OA model was induced in WT mice, followed by local injection of GapmeR-Eldr or GapmeR-scrambled control at 7, 14 and 21 days after surgery (Figure 7A). The in vivo cartilage targeted ability of the GapmeR was monitored in real time (Figure 7B). Furthermore, Cy3-labeled GapmeR-Eldr analysis showed that Eldr could penetrate cartilage (Figure S7A). Local delivery of GapmeR-Eldr remarkably protected the structure of cartilage as determined by gross appearance (Figure 7C), histological assessments (Figure 7C and Figure S7B) and radiographic (Figure 7D and Figure S7C), indicating that silencing of Eldr had a protective effect against surgically induced OA. Conversely, mice treated with GapmeR-scrambled control developed severe osteoarthritic phenotype (Figure 7C and Figure 7D). At a molecular level, Eldr knockdown in knee joints of DMM-operated mice attenuated IHH signaling (Figure 7E and Figure S7D), thereby inhibiting both inflammatory SASP factors and cellular senescence in cartilage (Figure 7F and Figure S7E). Compared with GapmeR-Eldr treating group, shorter telomeres were observed in PBS and GapmeR-scrambled control groups (Figure 7G), suggesting that Eldr promotes telomeric loss and causes premature aging. In addition, the chondrocyte proliferation was investigated by the EdU (Figure 7H). In pain-related behavioral tests, mice receiving GapmeR-Eldr injection exhibited higher pain thresholds (Figure 7I), indicating that silencing of Eldr in OA knee joints not only ameliorated histological features, but also reduced pain, a prominent symptom affecting OA patients.

Intriguingly, to test the feasibility of ELDR-targeting therapy in clinical OA, we evaluated the effect of ELDR antagonism in an explant culture of cartilage from OA patients undergoing

total knee arthroplasty (Figure 7J). ELDR inhibition in OA-affected tissue explants augmented the amount of anabolic markers and suppressed the expression of senescence markers and catabolic mediators (Figure 7K, Figure 7L and Figure S7F). Moreover, TUNEL staining showed remarkably decreased chondrocyte apoptosis in cartilage explants treated with GapmeR-ELDR (Figure 7M). Collectively, these data support a crucial role for ELDR in chondrocyte senescence and OA pathogenesis and demonstrate that therapeutic targeting of ELDR could elicit clinically desirable effects.

Discussion

The present study, to the best of our knowledge, is the first to elucidate the pivotal role of ELDR in chondrocyte senescence and cartilage degradation, adding new support for how dysregulated ELDR can drive distinct senescent phenotypes in vivo. The data from mice and human studies indicate increased activation of hedgehog signaling in OA, and that the use of hedgehog signaling inhibitors could attenuate the severity of OA or even prevent its development[33,42]. Furthermore, aberrantly high IHH signaling has previously been shown to promote aging[43,44]. Importantly, our results reveal that local IA administration of GapmeR-Eldr in mice substantially inhibits chondrocyte senescence and SASP by silencing hedgehog signaling, thereby ameliorating OA. Similar results were also found in human osteoarthritic cartilage explants. These findings provide in-depth mechanistic and translational insights into hedgehog pathway and could ultimately develop senolytic therapy for age-associated and post-traumatic OA treatment, moving beyond symptomatic relief to DMOADS.

Similar to pre-mRNA, non-coding exons in LncRNAs also undergo alternative splicing, a ubiquitous regulatory mechanism of gene expression[53,54], to produce different isoforms, which have specific expression patterns in human diseases. Furthermore, unlike protein-coding exons, almost all non-coding exons were found to be alternatively spliced, indicating that splicing patterns in lncRNAs may be different from those in protein-coding genes; as the requirement to maintain an open reading frame (ORF) is not imposed on non-coding RNA[45]. In this study, a novel transcript of ELDR (2724nt) formed by exons 1, 3 and 4 was identified in human chondrocytes, whereas two transcripts of ELDR included in database, 470nt and 2941nt, were not detected in our experiment. These findings indicate that this novel transcript may be required for

human chondrocyte in the context of physiologically normal and OA states. The molecular mechanisms underlying the ELDR gene alternative splicing in human chondrocytes should be extensively investigated in future studies, probably offering hope for combating OA using splicing modulation.

Unlike transcription factors, hnRNPL and KAT6A proteins lack putative DNA-binding motifs, so the mechanisms by which hnRNPL and KAT6A orient themself to their target sites across the chromatin remain unclear. The potential of RNA to bind to complementary DNA sequences has led to the hypothesis that lncRNAs could play crucial guiding roles in the establishment and transmission of chromatin states[21,37]. In our study, ELDR can act as a scaffold to bring hnRNPL and KAT6A proteins to specific histone modifications loci of IHH promoter through the formation of a RNA-DNA triplex, which further explains why chromatin-modifying complexes can bind to numerous gene promoters in a sequence-specific manner with limited binding domains.

Cellular senescence, a process that imposes permanent proliferative arrest on cells in response to various stressors, is a largely epigenetically determined cellular event[14,46]. It should be noted that LncRNAs have emerged in recent years as key epigenetic regulators of diverse cellular processes and can regulate gene expression in cis or in trans[22,37]. The central finding of our study is that epigenetic modifiers and transcription factor co-regulate hedgehog signaling pathway involved in chondrocyte senescence in the context of high level of ELDR. Our mechanistic study shows that exon 4 of ELDR recruits hnRNPL and KAT6A proteins to the histones of IHH promoter region and increases H3K4me3 and H3K9ac levels, which creates an open chromatin region in its promoter[47,48], enabling NRF1 to bind and thus modulating hedgehog signaling. These findings imply that ELDR determines the specific interaction of hnRNPL and KAT6A as a multi-protein modified complex to execute a unique transcriptional regulatory role of NRF1 in the regulation of hedgehog signaling and chondrocyte senescence, highlighting the highly dynamic nature of the epigenome during OA[7]. Targeting the epigenetic alterations observed in senescent cells holds great therapeutic prospects due to the reversible nature of epigenetic mechanisms[49,50]. The importance of aberrant chromatin state of senescent chondrocytes will therefore give an impetus for the clinical development of epigenetic therapies aimed at resetting the histone modifications imbalance observed in OA.

In summary, our study reveals a previously uncharacterized epigenetic switch for transcriptome reprogramming in chondrocyte senescence and cartilage degradation. The discovery of a lncRNA-mediated regulatory axis in aging and injury-induced chondrocyte senescence could shed light on the complex interactions between epigenetic modifiers and transcription factors, underscoring the finely tuned regulatory mechanisms that contribute to chondrocyte homeostasis physiologically and the susceptibility to senescence pathologically. Therefore, synthetically engineered ELDR containing the functional domains that act on the active regions of hedgehog signaling proteins can be tested for their therapeutic effects on OA, which could thereby offer opportunities to develop RNA-based senolytic agents in a cell-type specific manner, representing a new paradigm for OA therapy.

Methods

Human subjects

A total of 105 human OA and 53 normal cartilage were obtained from individuals undergoing knee arthroplasty and patients who underwent amputation surgery, respectively. The cartilage was immediately snap-frozen in liquid nitrogen. The specimens were further processed for histological examination and were categorized according to the modified Mankin scoring system[51]. This study protocol was approved by the ethics committee of xxxx, and full written consents were obtained before the operative procedure.

Inducible cartilage-specific conditional Eldr knockout and transgenic mice construction

$Eldr^{flox}$ mice were generated by Biocytogen using CRISPR/Cas9 based EGE system. After scanning the Eldr gene structure, transcripts, regulatory region, and conservation, the exons 4-6 of Eldr could be conditionally knockout. Single guide RNAs (sgRNAs) were designed to target the introns 3-4 and the introns 6-7, using the CRISPR design tool (http: //www.sanger.ac.uk/htgt/wge/). Candidate sgRNAs were screened for on-target activity using the UCA kit (Beijing Biocytogen), and two sgRNA with high specificity and on-target activity were chosen for the next step. The targeting vector was composed of a 1.5kb 3' homologous arm, Eldr exons 4-6 flanked by loxP and a 1.5kb 5'homologous arm. The targeting vector, the in vitro-synthesized sgRNAs and Cas9 mRNA were co-injected into C57BL/6 mouse zygotes. After

injection, surviving zygotes were then transferred into KM albino pseudopregnant. The obtained $Eldr^{flox}$ founder mice were validated by PCR amplification and DNA sequencing. Heterozygous $Eldr^{flox/+}$ mice were obtained by crossing the founder mice and the wildtype C57BL/6 mice. Genotyping of F1 heterozygous $Eldr^{flox/+}$ mice were confirmed by PCR amplification, DNA sequencing and southern blot analysis. Col2a1-$CreER^{T2}$ mice were purchased from Jackson Laboratories (Bar Harbor, ME, USA). To generate Col2a1-$CreER^{T2}$;$Eldr^{flox/flox}$ mice, $Eldr^{flox/flox}$ mice were mated with Col2a1-$CreER^{T2}$ mice to produce Col2a1-$CreER^{T2}$;$Eldr^{flox/+}$ mice, which were then mated with $Eldr^{flox/flox}$ mice.

Eldr ROSA26 KI mice were generated by Biocytogen using CRISPR/Cas9 based EGE system. After scanning the ROSA26 gene structure and transcripts. CAG promoter-loxP-STOP-loxP-mouse Eldr (NR_110421.1)-bGH polyA could be knockin into ROSA26. Single guide RNAs (sgRNAs) were designed to target the ROSA26 site, using the CRISPR design tool (http://crispr.mit.edu/). Candidate sgRNAs were screened for on-target activity using the UCA kit (Beijing Biocytogen), and the sgRNA with high specificity and on-target activity was chosen for the next step. The targeting vector was composed of a 1.8kb 3' homologous arm, GAG promoter, loxP-STOP-loxP-Mouse Eldr (NR_110421.1), bGH polyA and a 1.8kb 5'homologous arm. Next, the targeting vector, the in vitro-synthesized sgRNA and Cas9 mRNA were co-injected into C57BL/6 mouse zygotes. After injection, surviving zygotes were then transferred into KM albino pseudopregnant. The obtained ROSA26-LSL-$Eldr^{Mut}$ founder mice were validated by PCR amplification and DNA sequencing. Heterozygous ROSA26-LSL-$Eldr^{Mut/+}$ mice were obtained by crossing the founder mice and the wildtype C57BL/6 mice. Genotyping of F1 heterozygous ROSA26-LSL-$Eldr^{Mut/+}$ KI mice were confirmed by PCR amplification, DNA sequencing and southern blot analysis. We crossed Col2a1-$CreER^{T2}$ mice with ROSA26-LSL-$Eldr^{Mut/+}$ KI mice to obtain Col2a1-$CreER^{T2}$;$Eldr^{+/+}$KI mice. All mice were housed under pathogen-free conditions with five or fewer mice per cage. Mice had free access to food and water. The mice used for all experiments were randomly assigned to control or treatment groups and to those used in OA evaluation. The experimental protocol was approved by and performed in accordance with protocols from the Institutional Animal Care and Use Committee of xxxxx.

LncRNA-mRNA microarray analysis and bioinformatics analysis

Arraystar Human LncRNA Microarray V4.0, which is designed for the global profiling of human LncRNAs and protein-coding transcripts, was used. About 40,173 LncRNAs and 20,730 coding transcripts can be detected. Sample labeling and array hybridization were performed according to the Agilent One-Color Microarray-Based Gene Expression Analysis protocol (Agilent Technology) with minor modifications. Briefly, mRNA was purified from total RNA after removal of rRNA (mRNA-ONLY™ Eukaryotic mRNA Isolation Kit, Epicentre). Then, each sample was amplified and transcribed into fluorescent cRNA along the entire length of the transcripts without 3' bias utilizing a random priming method (Arraystar Flash RNA Labeling Kit, Arraystar). The labeled cRNAs were purified by RNeasy Mini Kit (Qiagen). 1μg of each labeled cRNA was fragmented by adding 5μl 10 × Blocking Agent and 1μl of 25 × Fragmentation Buffer, then heated the mixture at 60°C for 30min, finally 25μl 2×GE Hybridization buffer was added to dilute the labeled cRNA. 50μl of hybridization solution was dispensed into the gasket slide and assembled to the LncRNA expression microarray slide. The slides were incubated for 17 hours at 65°C in an Agilent Hybridization Oven. The hybridized arrays were washed, fixed and scanned with using the Agilent DNA Microarray Scanner (part number G2505C). Differentially expressed LncRNAs and mRNAs with statistical significance between the two groups were identified through Volcano Plot filtering. Differentially expressed LncRNAs and mRNAs between the two samples were identified through Fold Change filtering. Hierarchical clustering and GSEA analysis was implemented by R Package. Pathways of differentially expressed genes were analyzed by the KEGG database (http://www.kegg.jp/kegg/) and KOBAS software. The secondary structure of ELDR and ELDR binding motifs in IHH promoter were predicted by RNAfold and LongTarget, respectively. To evaluate the chromatin accessibility landscape of IHH gene promoter, ATAC-seq data for human catilage/chondrocyte from Cristrome Data Browser was analyzed (GSM2895180, GSM2895184, GSM2895186, GSM2895188, GSM2895190, GSM2895179, GSM2895183, GSM2895185, GSM2895187 and GSM2895189). With respect to histone histone modifications of IHH promoter, ChIP-seq data for H3K4me3, H4K3me1 and H3K9ac from Cristrome Data Browser was analyzed (GSM670034, GSM670004, GSM669990, GSM670024, GSM670000, GSM669927, GSM670030 and GSM669917).

Solexa sequencing

Total RNA from cartilage samples (3 wild type mice vs 3 ELDR cKO mice; 3 wild type mice vs 3

ELDR cKI mice) was quantified using a NanoDrop ND-100 instrument. 1-2 ug total RNA was used to prepare the sequencing library in the following steps: 1. Total RNA is enriched by oligo (dT) magnetic beads (rRNA removed); 2. RNA-seq library preparation using KAPA Stranded RNA-Seq LibraryPrep Kit (Illumina), whic h incorporates dUTP into the second cDNA strand and renders the RNA-seq library strand specific. The completed libraries were qualified with Agilent 2100 Bioanalyzer and quantified by absolute quantification qPCR method. To sequence the libraries on the Illumina HiSeq 4000 instrument, the barcoded libraries were mixed, denatured to single stranded DNA in NaOH, captured on Illumina flow cell, amplified in situ, and subsequently sequenced for 150 cycles for both ends on Illumina HiSeq instrument.

Image analysis and base calling were performed using Solexa pipeline v1.8 (off-Line Base Caller software, v1.8). Sequence quality was examined using the FastQC software. The trimmed reads (trimmed 5', 3'-adaptor bases using cutadapt) were ligned to reference genome using Hisat2 software. The transcript abundances for each sample was estimated with StringTie, and the FPKM value for gene and transcript level were calculated with R package Ballgown. The differentially expressed genes and transcripts were filtered using R package Ballgown. The novel genes and transcripts were predicted from assembled results by comparing to the reference annotation using StringTie and Ballgown, then use CPAT to assess the coding potential of those sequences. Principle Component Analysis (PCA) and correlation analysis were based on gene expression level. Hierarchical Clustering, Gene Ontology, Pathway analysis, scatter plots and volcano plots were performed with the differentially expressed genes in R, Python or shell environment for statistical computing and graphics. With respect to genes expression profiles in these two conditions, we found 87 up-regulated genes and 158 down-regulated genes in first condition (WT vs ELDR cKO), and 84 up-regulated genes and 153 down-regulated genes in second condition (WT vs ELDR cKI). A total of 4 genes were up-regulated in first condition and down-regulated in second condition. In contrast, a total of 7 genes were down-regulated in first condition and up-regulated in second condition.

Chromatin immunoprecipitation sequencing (ChIP-Seq)

For ChIP-Seq, chromatin was sonicated in a Corvaris sonicator to shear the genomic DNA to 150~500 bp. The sonicated sample lysates were subsequently spun at 13,000 rpm for 10 min in a

4℃ to remove debris; the supernatants were diluted 5 times with dilution buffer (0.01% SDS, 1% Triton X-100, 1.2mM EDTA pH8.0, 150nM NaCl). The primary antibodies (anti-hnRNPL and anti-KAT6A) were then added into the solution and rotated at 4℃ overnight. A total of 30 ul of Dynabeads Protein G beads (Life Technologies) were added and rotated at 4℃ for 4 hours. The beads were then washed eight times with 1 xlysis/wash buffer followed by 2 times wash in cold TE buffer. DNA molecules were reverse crosslinked by 130 mM NaHCO3, 1% SDS and were shaked on a vortex for 15 mins and incubated at 65℃ overnight. Library generation was performed using pooled ChIP DNA samples from three independent ChIP preparations using the Illumina protocol.

SA-ß-galactosidase staining

SA-β-gal staining was performed as previously described method[2,19]. Briefly, chondrocytes were washed twice with PBS and fixed with 2% PFA and 0.2% glutaraldehyde for 5min. Fixed cells were washed and incubated at 37°C for 12 to 16h in SA-β-gal staining solution. After incubation, the cells were washed with PBS twice and methanol followed by air drying. Total cells and SA-β-gal-positive cells were counted in three random fields per culture dish.

Telomere length measurement and Telomere FISH

Genomic DNA was extracted directly from chondrocytes using a Mini Genomic DNA Kit (QIAamp DNA Mini Kits) according to manufacturer's protocols (Qiagen). Telomere length was determined by using a RT-qPCR method. Telomere FISH was performed by using a PNA probe (Panagene). Briefly, chondrocytes were added to a six-well culture plates with glass slides and incubated at 37°C for 2h. Adhered cells were swollen in KCl buffer, fixed in methanol/acetic acid (3:1), rehydrated in PBS, fixed in 4% formaldehyde and then dehydrated in a series of concentrations of ethanol. Slides were incubated with hybridization mixture (70% formamide, 10mM $NaHPO_4$, pH 7.4, 10 mM NaCl, 20mM Tris buffer, pH 7.5), placed on a 80℃ heating block for 5min to denature chromosomal DNA and incubated with the PNA probe for 2h at room temperature. After washing, slides were mounted with Vectashield mounting medium containing DAPI (Vector Labs) and analyzed with a confocal microscope. For telomere FISH signals quantification, the custom software module Telometer, developed at the Johns Hopkins School of Medicine (the program and documentation are freely available for download at http:// demarzolab.pathology.jhmi.edu/telometer/index.html) was used. This software serves as a plugin

for use with the open-source image analysis program ImageJ (freely downloadable at https://imagej.nih.gov/ij/). After following the software's step-by-step instructions, remove the background signals from each image (DAPI and telomere). Select individual or multiple cells by hand from the DAPI image. The program will then generate values for the fluorescence intensities and areas of all Cy3 signals (telomeres) and DAPI signals (nuclei). The algorithm includes subtraction of background noise from the entire image, distinction of the individual telomere spots, and optional removal of halos and separation of conjoined telomeres. Further, the program generates signal intensity and area values for the entire region of the nucleus. Taking the ratio of the telomere 'sum' to the corresponding DAPI 'sum' serves to compensate for ploidy differences and the variation in the fraction of nuclei within the cutting plane of the section.

RNA in situ hybridization-proximity ligation assay (rISH-PLA)

The in situ proximity ligation assay (PLA) was performed on fixed primary proliferating chondrocytes using the DuoLink PLA fluorescence technology (Sigma-Aldrich#DUO92101) according to the manufacturer's protocol. About 3,000 chondrocytes were seeded per well of a 96-well plate and grown to a confluence of about 80%. Cells were fixed using 4% PFA for 7min at room Temperature. After two washing steps with PBS, cells were incubated with blocking solution in a humid chamber for 60 min at 37°C followed by incubation with primary antibodies (anti-hnRNPL and anti-KAT6A antibodies) for 1h at room temperature. PLA probe incubation, ligation, and signal amplification were performed according to the manufacturer's protocol. After two washing steps with PBS, DAPI was diluted 1:5000 in PBS and added to the cells for 5 min at room temperature. Interaction between ELDR and hnRNPL or KAT6A was confirmed using the rISH-PLA assay. The oligonucleotides against ELDR were designed using the Stellaris design tool (https://www.biosearchtech.com/support/education/stellaris-rna-fish)(Cy3-CAGCAAAAAAATG AGTGCCCTA).

Cell culture and transfection

Primary chondrocytes were isolated from human cartilage (OA and normal controls) and Col2a1-CreER^{T2};Eldr$^{flox/flox}$, Eldr$^{flox/flox}$, Eldr KI and Eldr cKI mice. Chondrocytes, SW1353 and C28/I2 cells were maintained as a monolayer in high glucose Dulbecco′s modified Eagle′s medium (DMEM) with 10% fetal calf serum (FCS), 100 IU/ml penicillin and 100µg/ml streptomycin at 37°C in an atmosphere of 5% CO_2. First-passage chondrocytes at 85% confluence

were used for all experiments. Human chondrocytes, SW1353 or C28/I2 cells were transfected with antisense LNA™ GapmeR-ELDR or antisense LNA™ GapmeR control labeled or unlabeled with Cy3 at 10mM using Lipofectamine RNAiMAX Transfection Reagent (Invitrogen, Life Technologies, Carlsbad, CA, USA). The ELDR sequence was synthesized and sub-cloned into the pCDNA3.1 (Invitrogen) vector. Overexpression of ELDR, hnRNPL or KAT6A was achieved via pCDNA3.1-ELDR, hnRNPL or KAT6A transfection, with an empty pCDNA3.1 vector used as a control (Invitrogen). Negative control siRNA or siRNA against hnRNPL and KAT6A (Sigma-Aldrich, St. Louis, MO, USA) was transfected into chondrocytes at a concentration of 50nM using Lipofectamine RNAiMAX Transfection Reagent (Invitrogen, Life Technologies, Carlsbad, CA, USA).

RNA isolation, cDNA synthesis and RT-qPCR

Total RNA from cartilage tissues and cultured cells was isolated using TRIzol reagent (Ambion, Life Technologies). RNA quantity and quality were determined using a nanodrop (Thermo Scientifific, Waltham, MA, USA) and Bioanalyzer (Agilent Inc., Santa Clara, CA, USA). RNA was then reverse-transcribed using the PrimeScript RT Reagent Kit (Takara Bio). Quantitative polymerase chain reaction (PCR) amplification was performed with an ABI QuantStudio 5 (Applied Biosystem, Foster City, CA). Relative gene expression (ELDR and other genes, normalized to endogenous control gene β-actin or GAPDH) was calculated using the comparative Ct method formula $2^{-\Delta\Delta Ct}$. The primer sequences used in this study are listed in Supplementary Table 2.

Flow cytometry and 5-Ethynyl-2′-deoxyuridine (EdU) assay

Apoptosis was evaluated by staining cells with both Annexin V-FITC and PI according to the manufacturer′s instructions. Cells that were positively stained with Annexin V-FITC and negatively stained for PI were considered apoptosis. Cells that were positively stained for both Annexin V-FITC and PI were considered necrosis. The cells were stained with 5μL Annexin V-FITC and 10μL PI and then analyzed with EpicsAltra (Beckman Coulter, CA, USA) FCM. For EdU assay, chondrocytes were inoculated at a density of 2 $x10^5$ per well into 24-well plates and cultured at 37°C in 5% CO_2. A total of 50 μM of EdU (Sigma-Aldrich) was then added to each well for 2h. Next, cells were fixed with 4% formaldehyde for 15min, followed by permeabilization with 0.5% Triton X-100 for 20min at room temperature. After washing the cells

three times with PBS, 100μl of 1X Apollo reaction cocktail was added to each well for 30min at room temperature. Subsequently, the cells were stained with Hoechst 33258.

3′ and 5′ rapid amplification of cDNA ends (RACE)

The 5'-RACE and 3'-RACE analyses were performed to determine the transcriptional initiation and termination sites of LncELDR using a SMARTer™ RACE cDNA Amplification Kit (Clontech, Palo Alto, CA, USA) according to the manufacturer's instructions. In brief, RNA was isolated from human chondrocytes and 3'-and 5'-RACE-Ready cDNA were synthesized using SMARTScribe Reverse Transcriptase. Amplification was performed as follows: five cycles: 94°C 30s 72°C 3 min; five cycles: 94°C 30s 70°C 30s 72°C 3min; 25 cycles 94°C 30s 68°C 30 s 72°C 3min. The obtained band was gel purified and cloning with the linearized pRACE vector. The obtained band was then sequenced. The primer sequences used in this study are shown in Supplementary Table 2.

Nuclear-cytoplasmic RNA fractionation and fluorescence in situ hybridization for chondrocytes and cartilage

Cytoplasmic and nuclear RNA Isolation were performed using PARIS™ Kit (Invitrogen) following the manufacturer' s instruction. Briefly, chondrocytes were digested to individual cells with trypsin and the trypsin was inactivated with complete medium followed by centrifugation at 1200 r.p.m. for 5min. The cells were then collected, washed twice with ice-cold PBS and lysed with 500μl ice-cold cell fractionation buffer. Cells were gently re-suspend by vortex or pipetting and incubated on ice for 12min. Centrifuge samples 3min at 500g to separates the nuclear and cytoplasmic cell fractions. The RNA of cytoplasmic and nuclear was eluted with 50μl of 95°C elution solution. All fractionation steps were performed at 4°C or on ice. Purification and analysis of cytoplasmic and nuclear RNA were subsequently performed according to the protocol of RT-qPCR assay.

For FISH, chondrocytes were seeded, fixed with 4% paraformaldehyde, treated with 0.5% Triton in phosphate buffer saline (PBS), and prehybridized. The cells were hybridized with 10μM Cy3-labled ELDR, U6 and 18S rRNA probes overnight. The probes used in this study are listed in Supplementary Table 3.

Serial deletion analysis and site-directed mutagenesis

For in vitro transcription of biotin-labeled and unlabeled ELDR, full-length ELDR or mutant

ELDR, carrying various deletions, were cloned into the pcDNA3.1 vector for the RNA pull-down assays. The mutant ELDR RNAs were generated using a QuikChange Site-directed Mutagenesis Kit (Stratagene, La Jolla, CA, USA) according to the manufacturer's instructions. The serial 3' nested PCR primers with common 5' primers or serial 5' nested PCR primers with common 3' primers were used to amplify the serial deletion fragments of ELDR.

RNA pull down and RNA immunoprecipitation (RIP)

Full-length ELDR and antisense sequences were obtained using a Transcript Aid T7 High Yield Transcription Kit (Thermo Scientific). Then, the sequences were treated with RNase-free DNase I and purified with the GeneJET RNA purification kit (Thermo Scientific). RNA pull down assays were performed with the Magnetic RNA-Protein Pull down Kit (Thermo Scientific). Nuclear extracts were prepared with the NE-PER Nuclear Protein Extraction Kit (Thermo Scientific). Three micrograms of biotin-labeled RNA and 1mg of nuclear extract were used in each pull down assay. Enriched proteins were subjected to SDS-PAGE followed by western blot and mass spectrometry (Q Exactive mass spectrometer, Thermo Scientific).

The RIP assay was performed according to the manufacturer’s protocol (the EZ-Magna RIP kit, Millipore, MA, USA). Briefly, 1×10^7 chondrocytes were harvested and lysed with RIP lysis buffer with one freeze-thaw cycle. Cell extracts were co-immunoprecipitated, and the retrieved RNA was subjected to RT-qPCR analysis. Normal mouse IgG was used as the NC. For RT-qPCR analysis, U1 RNA was used as a non-specific control.

Northern blot and Northern blot and RNA-electrophoretic mobility shift (EMSA) assay

Total RNA was extracted from chondrocytes with standard TRIzol methods, and then subjected to electrophoresis with formaldehyde denaturing agarose gel. Samples were transferred to positively charged NC film (Beyotime Biotechnology) with 20×SSC buffer (3.0M NaCl and 0.3M sodium citrate, pH7.0), followed by ultraviolet crosslinking. Membranes were incubated with hybrid buffer at 65°C for 20h supplemented with digoxin-labelled RNA probes generated by in vitro transcription. Digoxin signals were detected with HRP-conjugated anti-digoxin antibody (Thermo Scientific). EMSA experiments were performed using a LightShift Chemiluminescent RNA EMSA Kit (Thermo Scientifific).

ChIP-qPCR and ChIRP-qPCR analysis

The ChIP experiments were performed in accordance with the manufacturer's instructions of the

EZ-Magna ChIP A/G kit (Millipore, Billerica, MA, USA). A total of 1×10^6 chondrocytes were fixed in 1% formaldehyde at room temperature for 10min, and the nuclei were isolated with nuclear lysis buffer supplemented with a protease inhibitor. The chromatin DNA was sonicated and sheared to lengths between 100 and 200bp. The sheared chromatin was immunoprecipitated at 4°C overnight using an anti-hnRNPL antibody (Abcam), anti-H3K4me3 antibody (Cell Signaling Technology), anti-KAT6A antibody (Cell Signaling Technology, ChIP), anti-H3K9ac antibody (Abcam), anti-H3K4me1 antibody (Abcam) or anti-NRF1 antibody (Cell Signaling Technology). Normal mouse IgG was used as the NC, and an anti-RNA pol II antibody (Millipore) was used as the positive control. The ChIP-qPCR primers are listed in Supplementary Table 2.

The Magna ChIRP RNA Interactome Kit was obtained from Millipore (Millipore, MA, USA) and used according to the manufacturer's instructions. Briefly, the probes were designed using a single-molecule FISH online designer, were biotin-labeled at the 3′end and were divided into an "odds" or an "even" groups. A total of 2×10^7 chondrocytes were cross-linked for each hybridization reaction. Then, the cell lysate was sonicated to shear the chromatin into 100-200bp fragments. The sonicated cell lysates were hybridized with a mixture of biotinylated DNA probes for 4h at 37°C. Then, the binding complexes were recovered using streptavidin-conjugated magnetic beads. Finally, DNA, RNA and protein were eluted and purified from the beads. The probes used in the ChIRP assay are listed in Supplementary Table 3.

FRET assay and CD spectroscopy

For FRET assays, 5-carboxytetramethylrhodamine (TAMRA)-labeled TFO and 5-carboxyfluorescein (FAM)-labeled TTS were generated and mixed in binding buffer (20mM HEPES pH 7.5, 10 mM $MgCl_2$, 50 mM Na-acetate) in a ratio of 1:5 (500 nM TTS:2500 nM TFO). The mixtures were incubated at 55°C for 10min, followed by 10h incubation at 37°C. The fluorescence wavelengths between 480 and 690nm were measured using a Molecular Device M5 Plate Reader. For the CD spectroscopy, a 1:1 mixture of ELDR ssRNA TFO (2.2μM) and TTS oligos (2.2μM) (corresponding to the IHH promoter sequences predicted to be associated with ELDR, 2.2μM each) in binding buffer was equilibrated at 30°C for 1h. Control ssRNA/PROX1 TTS and FENDRR TFO/PITX2 TTS were used as the negative and positive control, respectively. LongTarget was used to predict the TFOs and TTS. The measurements were performed on a Chirascan spectrometer (Applied Photophysics).

DNA pull down

Briefly, 600bp upstream of the IHH gene coding region was PCR amplified using biotinylated primers. This probe was then added into chondrocytes lysates and incubated at room temperature. Probe-protein complexes were precipitated with streptavidin-coupled DynaBeads (Thermo Fisher Scientific), and proteins were eluted with increasing NaCl concentrations (700mM). Enriched proteins were subjected to SDS-PAGE, followed by western blot and mass spectrometry (Q Exactive mass spectrometer, Thermo Scientific).

Dual luciferase activity assay

Luciferase assays were performed to analyze the interaction between IHH promoter and ELDR or NRF1. The indicated IHH promoter fragments (-2000bp to +200bp) were cloned into the pGL3 plasmid (Promega, Madison, WI, USA) and transfected into chondrocytes overexpressing ELDR or NRF1. The pGL3 vector was used as a negative control. A reporter plasmid containing Renilla luciferase was used as the standard reference. After 24 transfection, the luciferase activities were detected following the instruction of the Dual-Luciferase Reporter Assay System (Promega, WI, USA). Renilla luciferase intensity was normalized against Firefly luciferase intensity. All transfections were carried out in triplicate.

Mass spectrometry analysis

Chondrocytes were washed three times with cold PBS buffer and lysed in 10mL of hypotonic buffer at 4°C for 1h. After centrifugation, the debris was washed three times with 5mL of hypotonic buffer and dissolved in 1.5mL of lysis buffer at 4°C for 30min. The resulting supernatant was incubated with control or ELDR at 4°C for 1h, respectively. Subsequently, the protein-control or protein-ELDR complex was captured by incubating it with 2mg (200μL) of streptavidin beads at 4°C for 45 min. Denatured protein sample was resolved on SDS-PAGE gel, which was stained with Coomassie Brilliant Blue. The purified protein bands were cut out and digested with trypsin. LC-MS/MS analyses were performed on an EASY-nLC 1000 HPLC system (Thermo Scientific), which was directly interfaced with a Q Exactive mass spectrometer (Thermo Scientific). The analytical column was a AcclaimR PepMap RSLC column (50μm ID, 15 cm length, C18, 2μm, 100Å) (Thermo Scientific). The Q Exactive mass spectrometer was operated in the data-dependent acquisition mode using Xcalibur 2.2 SP1 software and there was a single full-scan mass spectrum in the orbitrap (300-2000 m/z, 70,000 resolution) followed by 20

data-dependent MS/MS scans at 27% normalized collision energy (HCD). The MS/MS spectra from each LC-MS/MS run were searched against the fasta files using Sequest HT and phosphoRS 3.0 modules in Proteome Discoverer software (Version PD1.4, Thermo Scientific, USA).

Molecular docking and molecular dynamics simulations

Based on the best docking conformation of hnRNPL or KAT6A-ELDR complex, molecular dynamics simulations was performed by AMBER16 software. Hydrogen atoms were added to initialize the complex using the leap module and default protonation states at neutral value were set to ionize the amino acids before the simulation. The TIP3P water model and AmberTools with AMBER ff99sb force field was carried out to generate complex topology files. Na^+ was added to make the complex system neutral, and the final salt concentration was 0.15M. With particle mesh Ewald (PME) method, the molecular dynamics simulation was executed with minimal distance of 0.1nm to the margin of the box under periodic boundary conditions. Using the Verlet leapfrog algorithm, bond lengths were all constrained and the integration time step was set to 2fs. Subsequently, hnRNPL or KAT6A-ELDR complex was restrained with a harmonic potential as the form $k(\Delta x)^2$ force constant was set to k=100kcal/mol $^{-1}$Å^{-2}. Finally, a 10ns MD simulation with a 2000ps time step was performed under the condition of 298k and 1atm for protein-ELDR complexes. A total number of 5000 snapshots extracted from last 10ns MD simulation trajectory was employed for the final average structure of hnRNPL or KAT6A-ELDR complex.

Immunoblotting

Protein lysates were prepared from cultured primary human chondrocytes using RIPA buffer supplemented with protease and phosphatase inhibitors. The BCA Protein Assay Kit (ThermoFisher Scientific) was used to determine the protein concentrations. Proteins were separated using 10% SDS-PAGE gels and then transferred to PVDF membrane. The membranes were subsequently probed with primary antibodies against Col II (1:1500, Abcam), Aggrecan (1:1000, Abcam, ab36861), ADAMTS5 (1:250, Abcam, ab41037), MMP13 (1:2000; Abcam, ab39012), IHH (1:1000, Abcam, ab52919), Ptch1 (1:500, Abcam, ab53715), Gli (1:1000, Cell Signaling Technology, 3538), $p16^{INK4a}$ (1:1000; Abcam, ab40803), p21 (1:1000, Cell Signaling Technology, 2947), p53 (1:1000, Cell Signaling Technology, 48818), IL-6 (1:500, Abcam, 6672), TNF-α (1:1000, Cell Signaling Technology, 11948), IL-1β (1:1000, Cell Signaling Technology, 12703), MMP3 (1:500, Cell Signaling Technology, 14351), EGFR (1:1000, Abcam, 52894),

hnRNPL (1:1000, Abcam, 264340), KAT6A (Cell Signaling Technology, 78462), NRF1 (Cell Signaling Technology, 46743), HMGB1 (1:500, Abcam, 18256) and beta-actin (1:2000, Cell Signaling Technology, 4967) in 5% BSA in TBS-T overnight at 4°C. After washing with TBS-T, the membranes were incubated with horseradish peroxidase (HRP)-linked anti-rabbit IgG (1:1000, Cell Signaling Technology, 7074) or HRP-linked anti-mouse IgG (1:1000, Cell Signaling Technology, 7076) for 2h. Immunocomplexes were visualized through chemiluminescence using an ECL kit (Amersham Biosciences). The uncropped blots are provided in Supplementary Figure 8.

Cell immunofluorescence

Chondrocytes were cultured and treated on coverslips in 24-well plates. They were sequentially incubated with 4% formaldehyde, 0.5% Triton X-100, 5% BSA in PBS, primary antibodies, $p16^{INK4a}$ (1:100; Abcam, ab211542), TNF-α (1:500; Abcam, ab1793), IL-6 (1:1000; Abcam, ab246703), IL-1β (1:100, Abcam, ab156791), MMP3 (1:250; Abcam, ab52915), hnRNPL (1:1000; Abcam, ab32680), KAT6A (1:500, Sigma-Aldrich, HPA065052) and Alexa Fluor 555 (1:100, Abcam, ab150078)- or Alexa Fluor 488 (1:1000, Abcam, ab150077)-conjugated secondary antibodies and DAPI (Invitrogen). The fluorescence was visualized under CarlZeiss LSM710 confocal microscope (CarlZeiss, Oberkochen, Germany). The percentage of positive cells was calculated by Image-Pro Plus 6.0.

Immunohistochemistry (IHC), immunofluorescence staining and TUNEL

Paraffin-embedded tissue sections were deparaffinized with xylene and rehydrated with an alcohol gradient and water. Sections were incubated with primary antibodies at room temperature for 1h and biotin-labelled secondary antibodies for 30min, and then stained with Vectastain ABC kit and DAB peroxidase substrate kit (Vector Laboratories). Terminal deoxynucleotidyl transferase (TdT) dUTP Nick-End Labeling (TUNEL) assay was performed according to manufacturer′s instructions (In Situ Cell Death Detection Kit, Fluorescein, Roche).

The establishment of mouse OA model and GapmeR-ELDR treatment

Before surgical establishment of OA, 8-week-old $Eldr^{flox/flox}$, Eldr cKO, $Eldr^{ROSA26}$ and Eldr cKI mice were injected intraperitoneally with tamoxifen (TM) (100 μg/g body weight, Sigma, St. Louis, MO, USA) daily for 5 days. A surgical procedure was then performed to establish an experimental OA model in 10-week-old mice. Under general anaesthesia, destabilizing the medial

meniscus (DMM) in the right knee joints was performed using a surgical microscope. Sham operations were also performed in WT, $Eldr^{flox/flox}$ and $Eldr^{ROSA26}$ mice by opening and exposing the structures of the right knee and then closing the skin incision without manipulating the joint tissue. For the aging experiments, we compared WT, $Eldr^{flox/flox}$, Eldr cKO, $Eldr^{ROSA26}$ and Eldr cKI mice at 6, 12 and 18 months. For evaluation of GapmeR-Eldr joint residence time and penetration, mice were injected with Cy3-GapmeR-scrambled control or Cy3-GapmeR-Eldr. Images were taken at 24, 48 and 72 hours after IA injection using an in vivo imaging system (IVIS, Perkin Elmer). The mice were euthanized after in vivo imaging, and knee joints were harvested for cartilage penetration analysis. In the therapeutic approach, GapmeR-Eldr or GapmeR-scrambled control at dose of 10 mg/kg was injected into the mice knee joint using a 33G needle and a micro-syringe (Hamilton). The mice were received the injection at 7, 14 and 21 days after DMM. Mice were sacrificed at 8 weeks after treatment and subjected to histopathological and radiographic analysis.

OA cartilage explants were harvested from femoral condyles of OA patients who underwent total knee arthroplasty. Briefly, the cartilage explants were cut into pieces of approximately 1 mm^3 in volume. The explants were then dispended into DMEM containing 10% FBS supplemented with GapmeR-ELDR (0.5μM), GapmeR-scrambled control (0.5μM) or PBS, which was changed every 2 days. After 2 weeks of incubation, cartilage explants were collected for histological evaluation.

X-ray and histological evaluation

Radiographs of mouse knee joints were obtained using the Faxitron MX20 X-ray system. The tissues were embedded in paraffin, sectioned and stained with hematoxylin-eosin (HE), masson staining, safranin O/fast green and immunohistochemical assay. Decalcified cartilage was stained with Safranin-O and scored using the OARSI grading system (grade 0-6)[52]. Synovitis (grade 0-3) was determined by Safranin-O and hematoxylin staining[53]. Osteophyte development was identified by Safranin-O staining, and osteophyte maturity was quantified as described previously[54,55].

Statistical analysis

All statistical analyses were performed using GraphPad Prism 8 (GraphPad Software Inc., La Jolla, CA, USA). Data are presented as mean ± SEM. For statistical analysis of the microarray data, a

two-tailed t-test with the Benjamini and Hochberg correction was used. Comparison of statistical difference between two experimental groups was determined by two-tailed unpaired Student’s t test or Mann-Whitney U-test. One-way ANOVA (for multiple groups) was used followed by the Tukey′s post hoc analysis or Dunnett's tests. A P value less than 0.05 was considered statistically significant.

References

1. Loeser RF, Collins JA, Diekman BO. Ageing and the pathogenesis of osteoarthritis. Nat Rev Rheumatol 2016; 12: 412-20.

2. Jeon OH, Kim C, Laberge RM, et al. Local clearance of senescent cells attenuates the development of post-traumatic osteoarthritis and creates a pro-regenerative environment. Nature Medicine 2017; 23: 775-81.

3. McCulloch K, Litherland GJ, Rai TS. Cellular senescence in osteoarthritis pathology. Aging Cell 2017; 16: 210-18.

4. Gorgoulis V, Adams PD, Alimonti A, et al. Cellular Senescence: Defining a path forward. Cell 2019; 179: 813-27.

5. Choi WS, Lee G, Song WH, et al. The CH25H-CYP7B1-RORalpha axis of cholesterol metabolism regulates osteoarthritis. Nature 2019; 566: 254-58.

6. Martel-Pelletier J, Barr AJ, Cicuttini FM, et al. Osteoarthritis. Nat Rev Dis Primers 2016; 2: 16072.

7. Richard D, Liu Z, Cao J, et al. Evolutionary selection and constraint on human knee chondrocyte regulation impacts osteoarthritis risk. Cell 2020; 181: 362-81.

8. Wallace IJ, Worthington S, Felson DT, et al. Knee osteoarthritis has doubled in prevalence since the mid-20th century. Proc Natl Acad Sci U S A 2017; 114: 9332-336.

9. Jeon OH, David N, Campisi J, .et al. Senescent cells and osteoarthritis: a painful connection. J Clin Invest 2018; 128: 1229-37.

10. He S, Sharpless NE. Senescence in health and disease. Cell 2017; 169: 1000-11.

11. Mokuda S, Nakamichi R, Matsuzaki T, et al. Wwp2 maintains cartilage homeostasis through regulation of Adamts5. Nat Commun 2019; 10: 2429.

12. Matsuzaki T, Alvarez-Garcia O, Mokuda S, et al. FoxO transcription factors modulate autophagy and proteoglycan 4 in cartilage homeostasis and osteoarthritis. Sci Transl Med 2018; 10: eaan0746

13. Ji Q, Zheng Y, Zhang G, et al. Single-cell RNA-seq analysis reveals the progression of human osteoarthritis. Ann Rheum Dis 2019; 78: 100-10.

14. Jeon OH, Wilson DR, Clement CC, et al. Senescence cell-associated extracellular vesicles serve as osteoarthritis disease and therapeutic markers. JCI Insight 2019; 4: e125019.

15. Batshon G, Elayyan J, Qiq O, et al. Serum NT/CT SIRT1 ratio reflects early osteoarthritis and chondrosenescence. Ann Rheum Dis 2020; 79: 1370-80.

16. Martínez-Zamudio RI, Roux PF, de Freitas JANLF, et al. AP-1 imprints a reversible transcriptional programme of senescent cells. Nat Cell Biol 2020; 22: 842-55.

17. Partridge L, Fuentealba M, Kennedy BK. The quest to slow ageing through drug discovery. Nat Rev Drug Discov 2020; 19: 513-32.

18. Pignolo RJ, Passos JF, Khosla S, et al. Reducing senescent cell burden in aging and disease. Trends Mol Med 2020; 26: 630-38.

19. Mercer TR, Mattick JS. Structure and function of long noncoding RNAs in epigenetic regulation. Nat Struct Mol Biol 2013; 20: 300-7.

20. Ulitsky I, Bartel DP. lincRNAs: genomics, evolution, and mechanisms. Cell 2013; 154: 26-46.

21. Batista PJ, Chang HY. Long noncoding RNAs: cellular address codes in development and disease. Cell 2013; 152: 1298-307.

22. Hu WL, Jin L, Xu A, et al. GUARDIN is a p53-responsive long non-coding RNA that is essential for genomic stability. Nat Cell Biol 2018; 20: 492-502.

23. Li L, van Breugel PC, Loayza-Puch F, et al. LncRNA-OIS1 regulates DPP4 activation to modulate senescence induced by RAS. Nucleic Acids Res 2018; 46: 4213-27.

24. Kumar P P, Emechebe U, Smith R, et al. Coordinated control of senescence by lncRNA and a novel T-box3 co-repressor complex. Elife 2014; 3: e02805.

25. Pearson MJ, Philp AM, Heward JA, et al. Long intergenic noncoding RNAs mediate the human chondrocyte inflammatory response and are differentially expressed in osteoarthritis cartilage. Arthritis Rheumatol 2016; 68: 845-856.

26. Liu Q, Zhang X, Dai L, et al. Long noncoding RNA related to cartilage injury promotes chondrocyte extracellular matrix degradation in osteoarthritis. Arthritis Rheumatol 2014; 66: 969-78.

27. Fu M, Huang G, Zhang Z, et al. Expression profile of long noncoding RNAs in cartilage from knee osteoarthritis patients. Osteoarthritis Cartilage 2015; 23: 423-42.

28. Karro JE, Yan Y, Zheng D, et al. Pseudogene.org: a comprehensive database and comparison platform for pseudogene annotation. Nucleic Acids Res 2007; 35: D55-D60.

29. Singer RA, Arnes L, Cui Y, et al. The long noncoding RNA paupar modulates PAX6 regulatory activities to promote alpha cell development and function. Cell Metab 2019; 30: 1091-106.
30. Storer M, Mas A, Robert-Moreno A, et al. Senescence is a developmental mechanism that contributes to embryonic growth and patterning. Cell 2013; 155: 1119-30.
31. Muñoz-Espín D, Serrano M. Cellular senescence: from physiology to pathology. Nat Rev Mol Cell Biol 2014; 15: 82-96.
32. Faust HJ, Zhang H, Han J, et al. IL-17 and immunologically induced senescence regulate response to injury in osteoarthritis. J Clin Invest 2020; 130: 5493-507.
33. Lin AC, Seeto BL, Bartoszko JM, et al. Modulating hedgehog signaling can attenuate the severity of osteoarthritis. Nat Med 2009; 15: 1421-25.
34. Song EK, Jeon J, Jang DG, et al. ITGBL1 modulates integrin activity to promote cartilage formation and protect against arthritis. Sci Transl Med 2018; 10: eaam7486.
35. Son YO, Kim HE, Choi WS, et al. RNA-binding protein ZFP36L1 regulates osteoarthritis by modulating members of the heat shock protein 70 family. Nat Commun 2019; 10: 77.
36. Yao RW, Wang Y, Chen LL. Cellular functions of long noncoding RNAs. Nat Cell Biol 2019; 21: 542-51.
37. Fatica A, Bozzoni I. Long non-coding RNAs: new players in cell differentiation and development. Nat Rev Genet 2014; 15: 7-21.
38. Baell JB, Leaver DJ, Hermans SJ, et al. Inhibitors of histone acetyltransferases KAT6A/B induce senescence and arrest tumour growth. Nature 2018; 560: 253-57.
39. Price BD, D'Andrea AD. Chromatin remodeling at DNA double-strand breaks. Cell 2013; 152: 1344-54.
40. Bartelt A, Widenmaier SB, Schlein C, et al. Brown adipose tissue thermogenic adaptation requires Nrf1-mediated proteasomal activity. Nat Med 2018; 24: 292-303.
41. Wang Y, Zhao X, Lotz M, et al. Mitochondrial biogenesis is impaired in osteoarthritic chondrocytes but reversible via peroxisome proliferator-activated receptor-γ coactivator 1α. Arthritis Rheumatol 2015; 67: 2141-53.
42. Alman BA. The role of hedgehog signalling in skeletal health and disease. Nat Rev Rheumatol 2015; 11: 552-60.

43. Scheffold A, Baig AH, Chen Z, et al. Elevated Hedgehog activity contributes to attenuated DNA damage responses in aged hematopoietic cells. Leukemia 2020; 34: 1125-34.
44. Templeman NM, Cota V, Keyes W, et al. CREB Non-autonomously controls reproductive aging through hedgehog/patched signaling. Dev Cell 2020; 54: 92-105.
45. Tilgner H, Jahanbani F, Blauwkamp T, et al. Comprehensive transcriptome analysis using synthetic long-read sequencing reveals molecular co-association of distant splicing events. Nat Biotechnol 2015; 33: 736-42.
46. Childs BG, Durik M, Baker DJ, et al. Cellular senescence in aging and age-related disease: from mechanisms to therapy. Nat Med 2015; 21: 1424-35.
47. Chen T, Dent SY. Chromatin modifiers and remodellers: regulators of cellular differentiation. Nat Rev Genet 2014; 15: 93-106.
48. Klemm SL, Shipony Z, Greenleaf WJ. Chromatin accessibility and the regulatory epigenome. Nat Rev Genet 2019; 20 :207-20.
49. Bates SE. Epigenetic therapies for cancer. N Engl J Med 2020; 383: 650-63.
50. Cavalli G, Heard E. Advances in epigenetics link genetics to the environment and disease. Nature 2019; 571: 489-99.
51. Yamasaki K, Nakasa T, Miyaki S, et al. Expression of MicroRNA-146a in osteoarthritis cartilage. Arthritis Rheum 2009; 60: 1035-41.
52. Son YO, Park S, Kwak JS, et al. Estrogen-related receptor gamma causes osteoarthritis by upregulating extracellular matrix-degrading enzymes. Nat Commun 2017; 8: 2133.
53. Rhee J, Park SH, Kim SK, et al. Inhibition of BATF/JUN transcriptional activity protects against osteoarthritic cartilage destruction. Ann Rheum Dis 2017; 76: 427-34.
54. Wei Y, Luo L, Gui T, et al. Targeting cartilage EGFR pathway for osteoarthritis treatment. Sci Transl Med 2021; 13: eabb3946.
55. Huang J, Zhao L, Fan Y, et al. The microRNAs miR-204 and miR-211 maintain joint homeostasis and protect against osteoarthritis progression. Nat Commun 2019; 10: 2876.

Figure legends

Figure 1. Systematic identification of senescence-associated lncRNAs in human osteoarthritis (OA)

(A) Overview of the lncRNA discovery pipeline from transcriptome analyses of cartilage from OA patients (n=3) and controls (n=3).

(B and C) Volcano plot illustrating the biological and statistical significance of differential LncRNA expression levels (B) and heat map depicting 38 differentially expressed LncRNAs (fold change >10 or <0.1, Benjamini-Hochberg-corrected p) (3 controls and 3 OA). RNA was isolated from human cartilage samples (C).

(D) Representative histopathological staining of normal and OA cartilage tissues. Scale bar, left, 500 μm; right, 200 μm. n=3 biological replicates for each condition. Quantification of cartilage degradation grade and synovitis score in normal (n=53) and OA (n=105) human cartilage and synovial tissues. ***P<0.001 by two-tailed unpaired Student's t-test.

(E) Real-time PCR analysis of ELDR in human cartilage samples and cultured primary human chondrocytes from OA and controls, respectively. ***P<0.001 by Mann-Whitney U test.

(F) Representative image of agarose gel electrophoresis and bidirectional sequencing of 5'-RACE and 3'-RACE products of ELDR in cultured human primary chondrocytes. The novel transcript of ELDR was identified in human chondrocytes, and it has polyA tail in 3'UTR.

(G) Coding ability analysis indicates that the novel transcript of ELDR transcribed from exons 1, 3 and 4 is a non-coding RNA. The other two transcripts of ELDR included in database are 470nt (transcribed from exons 1, 3 and a small part of 4) and 2941nt (transcribed from exons 1-4) (http://genome.ucsc.edu/cgi-bin/hgGateway).

(H-J) Real-time PCR analysis of $p16^{INK4a}$, TNF-α, IL-1β and IL-6 in human cartilage tissues from OA (n=105) and controls (n=53). ***P<0.001 by unpaired two-sample Student's t test (H). Dot plots demonstrating the expression of indicated markers for each cell cluster on the t-SNE map (I) and representative images of immunostaining of these genes in human cartilage tissues (J). Scale bar, 20μm. Quantification of $p16^{INK4a}$, TNF-α, IL-1β and IL-6-positive chondrocytes. ***P<0.001 by two-tailed unpaired Student's t-test.

(K and L) The primary human chondrocytes were cultured for 72 hours, and then the relative telomere length (T/S ratio) was detected (K). Representative fluorescence microscopy images of

telomere FISH analysis in cultured human primary chondrocytes and quantitative analysis (L). Scale bar, 10μm. ***P<0.001 by two-tailed unpaired Student's t-test.

(M) Representative images of SA-β-Gal staining of cultured human primary chondrocytes and quantification. Scale bar, 100μm. ***P<0.001 by two-tailed unpaired Student's t-test.

(N) Representative images of immunofluorescence of $p16^{INK4a}$ and IL-6 in cultured human primary chondrocytes and quantification. Scale bar, 50μm. ***P<0.001 by two-tailed unpaired Student's t-test.

Figure 2. Eldr regulates cartilage development and embryonic chondrocyte senescence

(A and B) The $Eldr^{Flox}$ (A) and Eldr ROSA26 KI (B) mice construction strategies and validation by PCR and Southern blot (F1 founder).

(C and D) Immunoblotting analysis of $p16^{INK4a}$, p21, p53 and SASPs (IL-6, TNF-α and MMP3) in cultured chondrocytes from $Eldr^{flox/flox}$, Eldr cKO, $Eldr^{ROSA26}$ and Eldr cKI mice embryo at E14.5 (C) and E18.5 (D). n=3 biological replicates per group.

(E and F) Immunofluorescence staining of $p16^{INK4a}$ (E) and p21 (F) in cartilage tissues from $Eldr^{flox/flox}$, Eldr cKO, $Eldr^{ROSA26}$ and Eldr cKI mice embryo at E14.5 and E18.5 and quantification, respectively. Scale bar, 50μm. n=3 mice/group. ***P<0.001 by two-tailed unpaired Student's t-test.

(G and H) Representative images of HE and Masson staining in cartilage tissues from $Eldr^{flox/flox}$, Eldr cKO, $Eldr^{ROSA26}$ and Eldr cKI mice embryo at E14.5 (G) and E18.5 (H).

Figure 3. Eldr contributes to aging and injury-induced chondrocyte senescence

(A-C) Representative images of immunofluorescence of $p16^{INK4a}$, IL-6 and MMP3 and SA-β-Gal staining in cultured chondrocytes from 6-month-old mice ($Eldr^{flox/flox}$, Eldr cKO, $Eldr^{ROSA26}$, Eldr cKI) (A), 12-month-old mice ($Eldr^{flox/flox}$, Eldr cKO, $Eldr^{ROSA26}$, Eldr cKI) (B) and 18-month-old mice ($Eldr^{flox/flox}$, Eldr cKO, $Eldr^{ROSA26}$, Eldr cKI) , respectively (C). Quantification of $p16^{INK4a}$, IL-6 and MMP3 and SA-β-Gal-positive chondrocytes as a proportion of total chondrocytes. Scale bar, 20μm. n=6 mice/group. ***P<0.001 by by one-way ANOVA test followed by Tukey's post hoc.

(D) Representative images of Safranin O staining of cartilage tissues from 6-month-old mice

(Eldr$^{flox/flox}$, Eldr cKO, Eldr^{ROSA26}, Eldr cKI) , 12-month-old mice (Eldr$^{flox/flox}$, Eldr cKO, Eldr^{ROSA26}, Eldr cKI) and 18-month-old mice (Eldr$^{flox/flox}$, Eldr cKO, Eldr^{ROSA26}, Eldr cKI) and histological score (Osteoarthritis Research Society International, OARSI and synovial inflammation). Scale bar, 50μm. n=6 mice/group. **P<0.01, ***P<0.001 by two-tailed unpaired Student's t-test.

(E) Representative images of immunostaining of p16^{INK4a}, IL-6 and MMP3 in cartilage tissues and SA-β-Gal staining in chondrocytes from the indicated groups (Eldr$^{flox/flox}$ and Eldr^{ROSA26} mice undergoing sham surgery; wild-type (WT), Eldr cKO and Eldr cKI mice subjected to DMM surgery) at 8 weeks post surgery. Quantitative analysis of p16^{INK4a}, IL-6, MMP3 and SA-β-Gal-positive chondrocytes. Scale bar, 50μm. n=6 mice/group. ***P<0.001 by one-way ANOVA test followed by Tukey's post hoc.

(F) Representative images of Alcian blue, HE and Safranin O/fast green staining in cartilage tissues from the indicated groups and histological score (OARSI and synovial inflammation). **P<0.01, ***P<0.001 by two-tailed unpaired Student's t-test. Scale bar, 50μm. n=6 mice/group.

(G) Immunohistochemistry of ki67, Col2a1 and MMP13 in cartilage tissues from mice (Eldr$^{flox/flox}$ and Eldr^{ROSA26} mice undergoing sham surgery; wild-type (WT), Eldr cKO and Eldr cKI mice subjected to DMM surgery) and quantification. Scale bar, 50μm. n=6 mice/group. *P<0.05, **P<0.01, ***P<0.001 by two-tailed unpaired Student's t-test.

(H) Chondrocytes apoptosis was assayed by flow cytometry in the indicated groups (Eldr$^{flox/flox}$ and Eldr^{ROSA26} mice undergoing sham surgery; wild-type (WT), Eldr cKO and Eldr cKI mice subjected to DMM surgery). n=6 mice/group.

(I) EdU analysis in cartilage sections from different experiment groups (Eldr$^{flox/flox}$ and Eldr^{ROSA26} mice undergoing sham surgery; wild-type (WT), Eldr cKO and Eldr cKI mice subjected to DMM surgery). Scale bar, 50μm. n=6 mice/group. **P<0.01, ***P<0.001 by two-tailed unpaired Student's t-test.

Figure 4. ELDR directly binds to IHH gene promoter sequence

(A and B) GSEA analysis for biological processes, molecular function and cellular component in ELDR cKO chondrocytes (A) and cKI chondrocytes (B), respectively.

(C) Real-time PCR analysis of FoxO1, HPIP, ERRγ, ITGBL1 and IHH in wild type, ELDR cKO

and cKI chondrocytes. n=6 biological replicates/group; ***P<0.001 by two-tailed unpaired Student's t- test.

(D) KEGG analysis demonstrating Hedgehog signaling pathway enriched in osteoarthritis (OA). The left panel indicates differentially expressed signaling pathways. In general, the left panel shows ten most differentially expressed signaling pathways. In the right panel, the color of dot indicates P value and the size of dot suggests the number of genes contained in the pathway that intersect with the input gene list.

(E) Immunoblotting analysis of IHH, Ptch1, Gli, $p16^{INK4a}$, TNF-α, IL-1β, IL-6, MMP13, ADAMTS5, HMGB1, Col II and Aggrecan in wild type, ELDR cKO and cKI chondrocytes. n=3 biological replicates/group.

(F and G) Representative images of fluorescence in situ hybridisation (FISH) analysis of the subcellular distribution of ELDR in chondrocytes (F) and nuclear fractionation analyses and qRT-PCR analyses of ELDR expression in the nucleus and cytoplasm (G). n=3 biological replicates/group. Scale bar, 10μm.

(H) Transcriptional activity of the IHH promoter was evaluated using sequential deletions and by examining the IHH promoter linked to Renilla luciferase activity. ***P<0.001 by two-tailed unpaired Student's t- test. n=n=6 biological replicates/group.

(I) Schematic demonstration of the potential ELDR binding sites in the IHH promoter.

(J) ChIRP analysis of ELDR-associated chromatin in human primary chondrocytes, SW1353 and C28/I2. Retrieved chromatin was quantified by qRT-PCR. n=6 biological replicates/group; ***P<0.001 by one-way ANOVA followed by Dunnett's tests for multiple comparison.

(K and L) Fluorescence resonance energy transfer (FRET) of a 5:1 mixture of TFO in ELDR with TTS in the IHH promoter sequences (K) and circular dichroism (CD) spectroscopy of a 1:1 mixture of TFO in ELDR with TTS in the IHH promoter sequences (L).

(M) The effects of overexpression of wild-type or site-directed mutagenesis of ELDR (1138-1152nt) on IHH level were analyzed using real-time PCR in human primary chondrocytes, SW1353 and C28/I2. n=6 biological replicates/group; ***P<0.001 by Mann- Whitney U test.

(N) IHH wild-type or mutated type (-476 to -453bp) with wild-type or site-directed mutagenesis of ELDR (1138-1152nt) were subjected to luciferase reporter assays in human primary chondrocytes. n=6 biological replicates/group; ***P<0.001 by one-way ANOVA followed by

Dunnett's tests for multiple comparison.

(O) EGFR regulates LncELDR at the transcriptional level. n=6 biological replicates/group; ***P<0.001 by two-tailed unpaired Student's t- test. EGFR siRNA #1, #2 and #3 were constructed. Then, we tested their the efficiency of silencing, and EGFR siRNA #2 was chosen for further analysis. pcDNA 3.1(+)-EGFR was constructed to overexpress EGFR. The chondrocytes were transfected with EGFR siRNA #2 or pcDNA 3.1(+)-EGFR using Lipofectamine 3000 transfection reagent (Invitrogen, USA). After 48 hours transfection, the related analysis was performed.

(P) The LncELDR promoter can be activated by EGFR. n=6 biological replicates/group; *P<0.05, **P<0.01 and ***P<0.001 by two-tailed unpaired Student's t- test.

(Q) EGFR bounds to E-boxes on the LncELDR promoter. n=6 biological replicates/group; ***P<0.001 by two-tailed unpaired Student's t- test.

Figure 5. ELDR/hnRNPL/KAT6A promotes H3K4me3 and H3K9ac of IHH promoter

(A-C) Representative image of silver-stained PAGE gels showing separated proteins that were pulled down using biotin-labeled ELDR and arrows indicate hnRNPL and KAT6A (A), further confirmed by mass spectrometry (B) and western blot analysis (C). The cultured human chondrocytes were employed.

(D) RNA in situ hybridization-proximity ligation assay (rISH-PLA) detects the close proximity of a specific RNA with proteins in situ. rISH-PLA confirms the proximity of ELDR to endogenous hnRNPL or KAT6A in the nucleus of cultured human primary chondrocyte. Scale bar, 10μm.

(E) RNA immunoprecipitation (RIP) analysis using the anti-hnRNPL or KAT6A antibody revealed that ELDR interacted with endogenous hnRNPL and KAT6A in cultured human primary chondrocytes and SW1353. U1 was used as the negative control. n=6 biological replicates/group ***P<0.001 by two-tailed unpaired Student's t-test.

(F and G) Serial deletions of ELDR were performed in the RNA pull-down assays to identify the core regions of ELDR for the physical interaction with hnRNPL and KAT6A (F). Silver staining image of proteins pulled down by the 5'-terminus of the truncated ELDR (1640-1680nt). The interaction between the truncated ELDR and hnRNPL or KAT6A was confirmed by RNA pull-down and western blotting with nuclear extract or purified recombinant hnRNPL and KAT6A.

hnRNPL and KAT6A proteins and biotin-labeled ELDR (1640-1680nt) probes were incubated for an EMSA assay (G). The cultured human chondrocytes were used.

(H) Four stable stem-loop structure of ELDR was predicted. WT and mutant ELDR were shown.

(I) Interaction model between ELDR (1640-1680nt) and hnRNPL or KAT6A.

(J) RIP analysis performed after site-directed mutagenesis of 1640-1680nt of ELDR in cultured human primary chondrocytes and SW1353. n=6 biological replicates/group; ***P<0.001 by two-tailed unpaired Student's t-test.

(K) ChIP-qPCR analysis of the hnRNPL and KAT6A genomic occupancy and H3K4me3 and H3K9ac in IHH promoter after overexpression or depletion of EDLR in cultured human primary chondrocytes. n=6 biological replicates/group; **P<0.01 by two-tailed unpaired Student's t-test.

(L) Real-time PCR analysis of IHH expression in the hnRNPL or KAT6A knockdown or overexpression or on ELDR-induced IHH expression in cultured human primary chondrocytes. n=6 biological replicates/group; *P<0.05, **P<0.01 and ***P<0.001 by two-tailed t-tests and one-way analyses of variance (ANOVA) followed by Dunnett's tests for multiple comparison.

Figure 6. ELDR/hnRNPL/KAT6A creates an open chromatin region in IHH promoter for NRF1 binding

(A and B) Heatmap of hnRNPL (A) and KAT6A (B) global genomic binding at the target sites in chondrocytes after transduction of control and GapmeR-ELDR.

(C and D) Heatmap demonstrating the expression change of hnRNPL/KAT6A co-occupied genes in chondrocytes after transfection of control and GapmeR-ELDR (C) and GSEA data showing the enrichment of ChIP-seq promoter peaks with significant loss of hnRNPL/KAT6A binding for the downregulated genes in chondrocytes after transfection of GapmeR-ELDR (D).

(E-G) ATAC-Seq analysis showing accessible chromatin region in IHH promoter in OA patients and motif enrichment analysis reveals a transcription factor (NRF1) relevant to OA (E), further confirmed by DNA pull down, western blot (F) and mass spectrometry (G)

(H and I) RT-qPCR analysis of NRF1 expression in cultured human primary chondrocytes from OA and controls (H). Immunostaining and quantification of NRF1 in cartilage tissues of the above-mentioned groups (I). n=6 mice/group; Scale bar, 20μm; **P<0.01; ***P<0.001 by two-tailed unpaired Student's t-test (I).

(J) ChIP-Seq analysis demonstrating that the enrichment of H3K4me3, H3K9ac and H3K4me1 in IHH promoter region. The ChIP analysis further confirmed high levels of H3K4me3, H3K9ac and H3K4me1 in human OA and control chondrocytes in the IHH promoter. n=6 biological replicates/group; ***P<0.001 by two-tailed unpaired Student's t-test.

(K) Co-IP analysis showing the relationships between NRF1 and hnRNPL or KAT6A in chondrocytes.

(L) ChIP-qPCR analysis of the NRF1 genomic occupancy in IHH promoter after overexpression or site-directed mutagenesis of EDLR in human primary chondrocytes and SW1353. n=6 biological replicates/group; ***P<0.001 by two-tailed unpaired Student's t-test.

(M) Using luciferase reporter assays and immunofluorescence, the interaction between NRF1 and IHH promoter was analyzed in different conditions. n=6 biological replicates/group. Scale bar, 20μm. In OA chondrocytes, ELDR, hnRNPL and KAT6A were highly expressed. Thus, ELDR recruits hnRNPL and KAT6A (as confirmed by cell immunofluorescence, i.e., the high co-expression of hnRNPL and KAT6A in the nucleus.) to IHH promoter and promotes its histone modifications, creating an open chromatin status in IHH promoter. As validated by luciferase activity assay, the chondrocytes were co-transfected by pcDNA-NRF1 and pGL3-IHH-WT and the result shows the increase of luciferase activity, indicating the interaction between NRFI and IHH promoter. In ELDR cKI +siRNAhnRNPL and siRNA KAT6A chondrocytes, although high level of ELDR, it can not recruit hnRNPL and KAT6A (as confirmed by cell immunofluorescence) and a closed chromatin status was produced in IHH promoter. As validated by luciferase activity assay, NRF1 can not bind its promoter. In ELDR cKO +pcDNA-hnRNPL and KAT6A chondrocytes, although high level of hnRNPL and KAT6A (as confirmed by cell immunofluorescence), they can not be recruited to the promoter of IHH due to very low level of ELDR. Therefore, the chromatin status of IHH promoter was closed, which precludes NRF1 binding IHH promoter. As validated by luciferase activity assay, NRF1 can not bind its promoter.

(N) Schematic model illustrating the ELDR/hnRNPL/KAT6A complex-mediated transcriptional regulatory model.

Figure 7. Pharmacological inhibition of ELDR in vivo attenuates chondrocyte senescence and cartilage degradation

(A) Study protocol for examining the effect of GapmeR-Eldr on chondrocyte senescence and cartilage degradation.

(B) In vivo time-dependent fluorescence image in mice at 24, 48 and 72 hours after the administration of Cy3-GapmeR-Eldr or its control.

(C and D) The cartilage degradation evaluated by Alcian blue, HE and Safranin O staining, gross appearance, X- ray and micro-CT in wild type mice subjected to DMM surgery followed by treatment with PBS, GapmeR-scrambled control and GapmeR-Eldr at indicated weeks. Osteoarthritis Research Society International (OARSI), osteophyte formation and synovial inflammation were also quantified respectively. n=6 mice/group. Scale bar, 100μm. **P<0.01 and ***P<0.001 by one- way ANOVA test followed by Tukey's post hoc.

(E) Representative images of immunostaining of IHH, Ptch1 and Gli in cartilage from the indicated groups of mice. Scale bar, 100μm. n=6 mice/group.

(F) Representative images of immunohistochemistry of $p16^{INK4a}$, IL-6 and MMP13 in cartilage and SA-β-Gal staining in chondrocytes from mice treated with PBS, GapmeR-scrambled control and GapmeR-Eldr, respectively. Scale bar, 50μm. n=6 mice/group.

(G) Representative fluorescence microscopy images of telomere FISH analysis and quantification in chondrocytes from mice undergoing PBS, GapmeR-scrambled control or GapmeR-Eldr treatment, respectively. Scale bar, 10μm. n=6 mice/group.

(H) EdU staining for chondrocytes from mice treated with PBS, GapmeR-scrambled control and GapmeR-Eldr, respectively. Scale bars, 50 μm. n=6 mice/group.

(I) Intra-articular injection of GapmeR-Eldr reduces pain sensitivity induced by chondrocyte senescence and cartilage degradation. The Von Frey test was performed in the 6- month- old mice receiving GapmeR-Eldr injection at the age of 8 weeks. n=6 mice/group. ***P<0.001 by one- way ANOVA test followed by Tukey's post hoc.

(J) Study protocol for ELDR-targeting therapy in clinical OA.

(K-M) Representative images of immunostaining of p16INK4a, IL-6, MMP13 and Col II in human OA cartilage treated with PBS, GapmeR-scrambled control or GapmeR-ELDR, respectively (K). Scale bars, 50 μm. Real-time PCR analysis of p16INK4a, IL-6, MMP13 and Col II (L). ***P<0.001 by one- way ANOVA test followed by Tukey's post hoc. TUNEL staining of human OA cartilage after PBS, GapmeR-scrambled control or GapmeR-ELDR treatment (M).

Scale bars, 20 μm. n=6 mice/group.

Figures

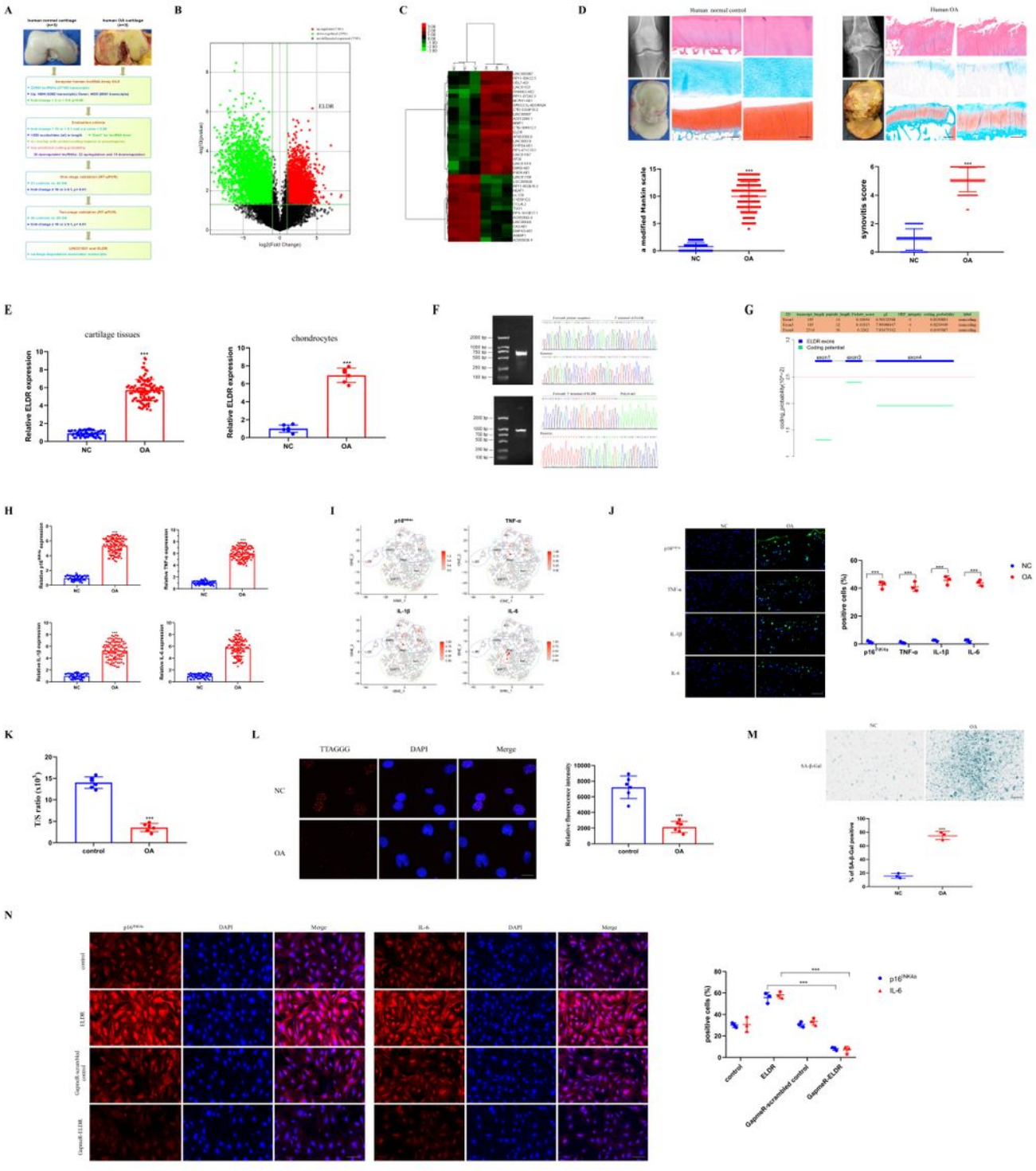

Figure 1

Systematic identification of senescence-associated lncRNAs in human osteoarthritis (OA)

(A) Overview of the lncRNA discovery pipeline from transcriptome analyses of cartilage from OA patients (n=3) and controls (n=3). (B and C) Volcano plot illustrating the biological and statistical significance of differential LncRNA expression levels (B) and heat map depicting 38 differentially expressed LncRNAs (fold change >10 or <0.1, Benjamini-Hochberg-corrected p) (3 controls and 3 OA). RNA was isolated from human cartilage samples (C).

(D) Representative histopathological staining of normal and OA cartilage tissues. Scale bar, left, 500 μm; right, 200 μm. n=3 biological replicates for each condition. Quantification of cartilage degradation grade and synovitis score in normal (n=53) and OA (n=105) human cartilage and synovial tissues. ***P<0.001 by two-tailed unpaired Student's t-test.

(E) Real-time PCR analysis of ELDR in human cartilage samples and cultured primary human chondrocytes from OA and controls, respectively. ***P<0.001 by Mann-Whitney U test.

(F) Representative image of agarose gel electrophoresis and bidirectional sequencing of 5'-RACE and 3'-RACE products of ELDR in cultured human primary chondrocytes. The novel transcript of ELDR was identified in human chondrocytes, and it has polyA tail in 3'UTR.

(G) Coding ability analysis indicates that the novel transcript of ELDR transcribed from exons 1, 3 and 4 is a non-coding RNA. The other two transcripts of ELDR included in database are 470nt (transcribed from exons 1, 3 and a small part of 4) and 2941nt (transcribed from exons 1-4) (http://genome.ucsc.edu/cgi-bin/hgGateway).

(H-J) Real-time PCR analysis of p16INK4a, TNF-α, IL-1β and IL-6 in human cartilage tissues from OA (n=105) and controls (n=53). ***P<0.001 by unpaired two-sample Student’s t test (H). Dot plots demonstrating the expression of indicated markers for each cell cluster on the t-SNE map (I) and representative images of immunostaining of these genes in human cartilage tissues (J). Scale bar, 20μm. Quantification of p16INK4a, TNF-α, IL-1β and IL-6-positive chondrocytes. ***P<0.001 by two-tailed unpaired Student's t-test.

(K and L) The primary human chondrocytes were cultured for 72 hours, and then the relative telomere length (T/S ratio) was detected (K). Representative fluorescence microscopy images of telomere FISH analysis in cultured human primary chondrocytes and quantitative 1 analysis (L). Scale bar, 10μm. ***P<0.001 by two-tailed unpaired Student's t-test.

(M) Representative images of SA-β-Gal staining of cultured human primary chondrocytes and quantification. Scale bar, 100μm. ***P<0.001 by two-tailed unpaired Student's t-test.

(N) Representative images of immunofluorescence of p16INK4a and IL-6 in cultured human primary chondrocytes and quantification. Scale bar, 50μm. ***P<0.001 by two-tailed unpaired Student's t-test.

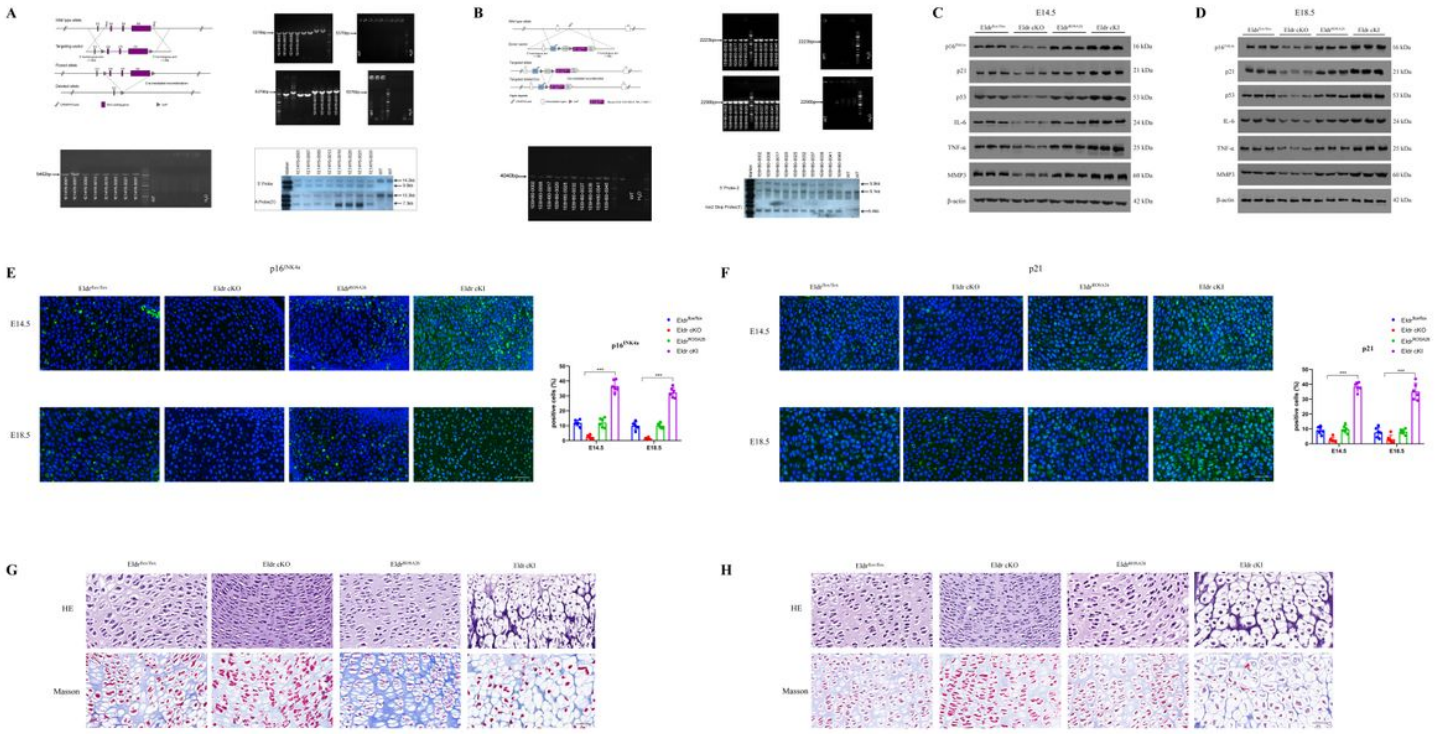

Figure 2

Eldr regulates cartilage development and embryonic chondrocyte senescence

(A and B) The EldrFlox (A) and Eldr ROSA26 KI (B) mice construction strategies and validation by PCR and Southern blot (F1 founder).

(C and D) Immunoblotting analysis of p16INK4a, p21, p53 and SASPs (IL-6, TNF-α and MMP3) in cultured chondrocytes from Eldrflox/flox, Eldr cKO, EldrROSA26 and Eldr cKI mice embryo at E14.5

(C) and E18.5 (D). n=3 biological replicates per group.

(E and F) Immunofluorescence staining of p16INK4a (E) and p21 (F) in cartilage tissues from Eldrflox/flox, Eldr cKO, EldrROSA26 and Eldr cKI mice embryo at E14.5 and E18.5 and quantification, respectively. Scale bar, 50μm. n=3 mice/group. ***P<0.001 by two-tailed unpaired Student's t-test.

(G and H) Representative images of HE and Masson staining in cartilage tissues from Eldrflox/flox, Eldr cKO, EldrROSA26 and Eldr cKI mice embryo at E14.5 (G) and E18.5 (H).

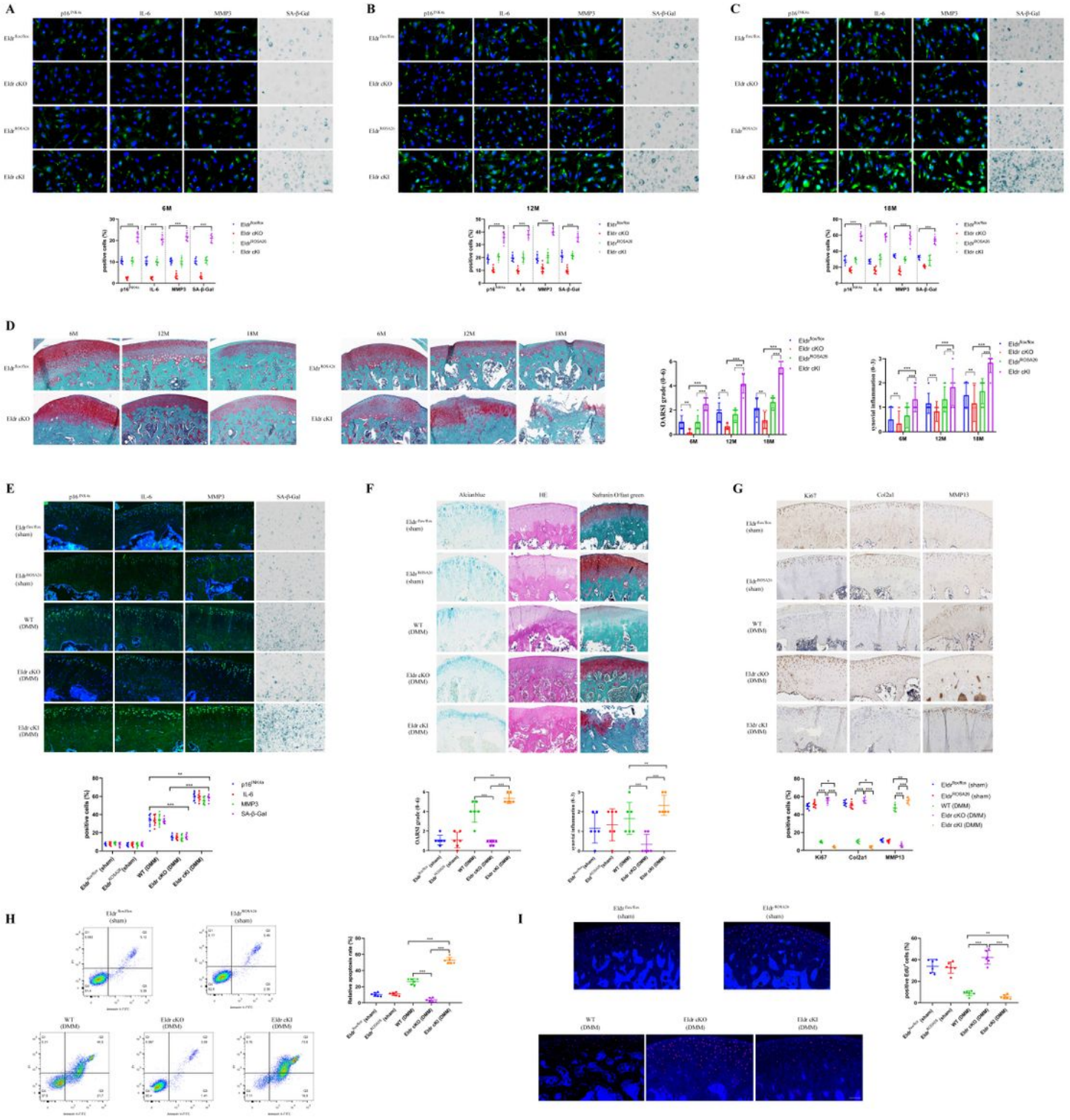

Figure 3

Eldr contributes to aging and injury-induced chondrocyte senescence

(A-C) Representative images of immunofluorescence of p16INK4a, IL-6 and MMP3 and SA-β-Gal staining in cultured chondrocytes from 6-month-old mice (Eldrflox/flox, Eldr cKO, EldrROSA26, Eldr cKI) (A), 12-month-old mice (Eldrflox/flox, Eldr cKO, EldrROSA26, Eldr cKI) (B) and 18-month-old mice (Eldrflox/flox,

Eldr cKO, EldrROSA26, Eldr cKI) , respectively (C). Quantification of p16INK4a, IL-6 and MMP3 and SA-β-Gal-positive chondrocytes as a proportion of total chondrocytes. Scale bar, 20μm. n=6 mice/group. ***P<0.001 by by one-way ANOVA test followed by Tukey's post hoc.

(D) Representative images of Safranin O staining of cartilage tissues from 6-month-old mice (Eldrflox/flox, Eldr cKO, EldrROSA26, Eldr cKI) , 12-month-old mice (Eldrflox/1 flox, Eldr cKO, EldrROSA26, Eldr cKI) and 18-month-old mice (Eldrflox/flox, Eldr cKO, EldrROSA26, Eldr cKI) and histological score (Osteoarthritis Research Society International, OARSI and synovial inflammation). Scale bar, 50μm. n=6 mice/group. **P<0.01, ***P<0.001 by two-tailed unpaired Student's t-test.

(E) Representative images of immunostaining of p16INK4a, IL-6 and MMP3 in cartilage tissues and SA-β-Gal staining in chondrocytes from the indicated groups (Eldrflox/flox and EldrROSA26 mice undergoing sham surgery; wild-type (WT), Eldr cKO and Eldr cKI mice subjected to DMM surgery) at 8 weeks post surgery. Quantitative analysis of p16INK4a, IL-6, MMP3 and SA-β-Gal-positive chondrocytes. Scale bar, 50μm. n=6 mice/group. ***P<0.001 by one-way ANOVA test followed by Tukey's post hoc.

(F) Representative images of Alcian blue, HE and Safranin O/fast green staining in cartilage tissues from the indicated groups and histological score (OARSI and synovial inflammation). **P<0.01, ***P<0.001 by two-tailed unpaired Student's t-test. Scale bar, 50μm. n=6 mice/group.

(G) Immunohistochemistry of ki67, Col2a1 and MMP13 in cartilage tissues from mice (Eldrflox/flox and EldrROSA26 mice undergoing sham surgery; wild-type (WT), Eldr cKO and Eldr cKI mice subjected to DMM surgery) and quantification. Scale bar, 50μm. n=6 mice/group. *P<0.05, **P<0.01, ***P<0.001 by two-tailed unpaired Student's t-test.

(H) Chondrocytes apoptosis was assayed by flow cytometry in the indicated groups (Eldrflox/flox and EldrROSA26 mice undergoing sham surgery; wild-type (WT), Eldr cKO and Eldr cKI mice subjected to DMM surgery). n=6 mice/group.

(I) EdU analysis in cartilage sections from different experiment groups (Eldrflox/flox and EldrROSA26 mice undergoing sham surgery; wild-type (WT), Eldr cKO and Eldr cKI mice subjected to DMM surgery). Scale bar, 50μm. n=6 mice/group. **P<0.01, ***P<0.001 by two-tailed unpaired Student's t-test.

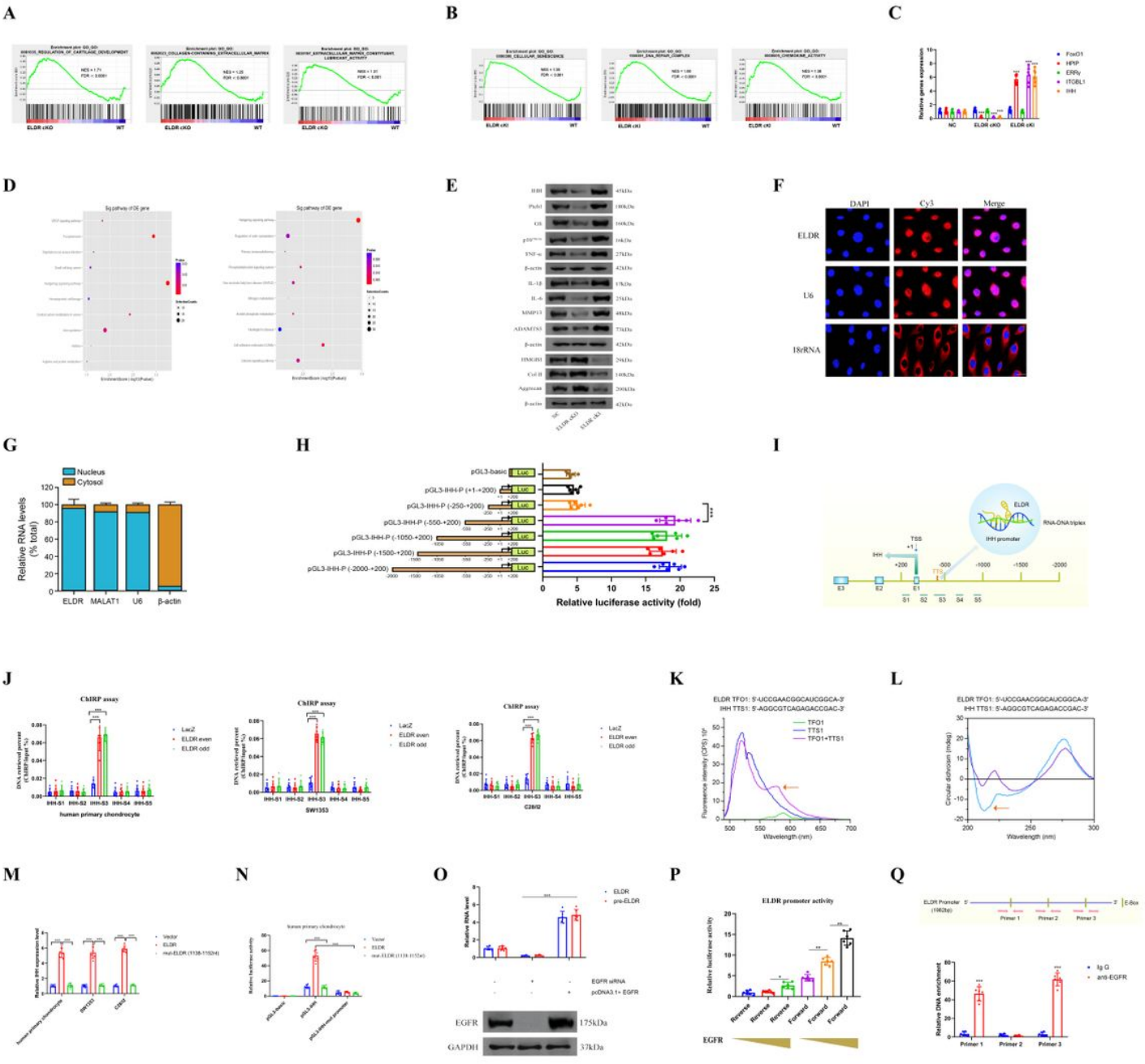

Figure 4

ELDR directly binds to IHH gene promoter sequence

(A and B) GSEA analysis for biological processes, molecular function and cellular component in ELDR cKO chondrocytes (A) and cKI chondrocytes (B), respectively.

(C) Real-time PCR analysis of FoxO1, HPIP, ERRγ, ITGBL1 and IHH in wild type, ELDR cKO and cKI chondrocytes. n=6 biological replicates/group; ***P<0.001 by two-tailed unpaired Student's t- test.

(D) KEGG analysis demonstrating Hedgehog signaling pathway enriched in osteoarthritis (OA). The left panel indicates differentially expressed signaling pathways. In general, the left panel shows ten most differentially expressed signaling pathways. In the right panel, the color of dot indicates P value and the size of dot suggests the number of genes contained in the pathway that intersect with the input gene list.

(E) Immunoblotting analysis of IHH, Ptch1, Gli, p16INK4a, TNF-α, IL-1β, IL-6, MMP13, ADAMTS5, HMGB1, Col II and Aggrecan in wild type, ELDR cKO and cKI chondrocytes. n=3 biological replicates/group.

(F and G) Representative images of fluorescence in situ hybridisation (FISH) analysis of the subcellular distribution of ELDR in chondrocytes (F) and nuclear fractionation analyses and qRT-PCR analyses of ELDR expression in the nucleus and cytoplasm (G). n=3 biological replicates/group. Scale bar, 10μm.

(H) Transcriptional activity of the IHH promoter was evaluated using sequential deletions and by examining the IHH promoter linked to Renilla luciferase activity. ***P<0.001 by two-tailed unpaired Student's t- test. n=n=6 biological replicates/group.

(I) Schematic demonstration of the potential ELDR binding sites in the IHH promoter.

(J) ChIRP analysis of ELDR-associated chromatin in human primary chondrocytes, SW1353 and C28/I2. Retrieved chromatin was quantified by qRT-PCR. n=6 biological replicates/group; ***P<0.001 by one-way ANOVAfollowed by Dunnett's tests for multiple comparison.

(K and L) Fluorescence resonance energy transfer (FRET) of a 5:1 mixture of TFO in ELDR with TTS in the IHH promoter sequences (K) and circular dichroism (CD) spectroscopy of a 1:1 mixture of TFO in ELDR with TTS in the IHH promoter sequences (L).

(M) The effects of overexpression of wild-type or site-directed mutagenesis of ELDR (1138-1152nt) on IHH level were analyzed using real-time PCR in human primary chondrocytes, SW1353 and C28/I2. n=6 biological replicates/group; ***P<0.001 by Mann-Whitney U test.

(N) IHH wild-type or mutated type (-476 to -453bp) with wild-type or site-directed mutagenesis of ELDR (1138-1152nt) were subjected to luciferase reporter assays in human primary chondrocytes. n=6 biological replicates/group; ***P<0.001 by one-way ANOVA followed by Dunnett's tests for multiple comparison.

(O) EGFR regulates LncELDR at the transcriptional level. n=6 biological replicates/group; ***P<0.001 by two-tailed unpaired Student's t- test. EGFR siRNA #1, #2 and #3 were constructed. Then, we tested their the efficiency of silencing, and EGFR siRNA #2 was chosen for further analysis. pcDNA 3.1(+)-EGFR was constructed to overexpress EGFR. The chondrocytes were transfected with EGFR siRNA #2 or pcDNA 3.1(+)-EGFR using Lipofectamine 3000 transfection reagent (Invitrogen, USA). After 48 hours transfection, the related analysis was performed.

(P) The LncELDR promoter can be activated by EGFR. n=6 biological replicates/group; *P<0.05, **P<0.01 and ***P<0.001 by two-tailed unpaired Student's t- test.

(Q) EGFR bounds to E-boxes on the LncELDR promoter. n=6 biological replicates/group; ***P<0.001 by two-tailed unpaired Student's t- test.

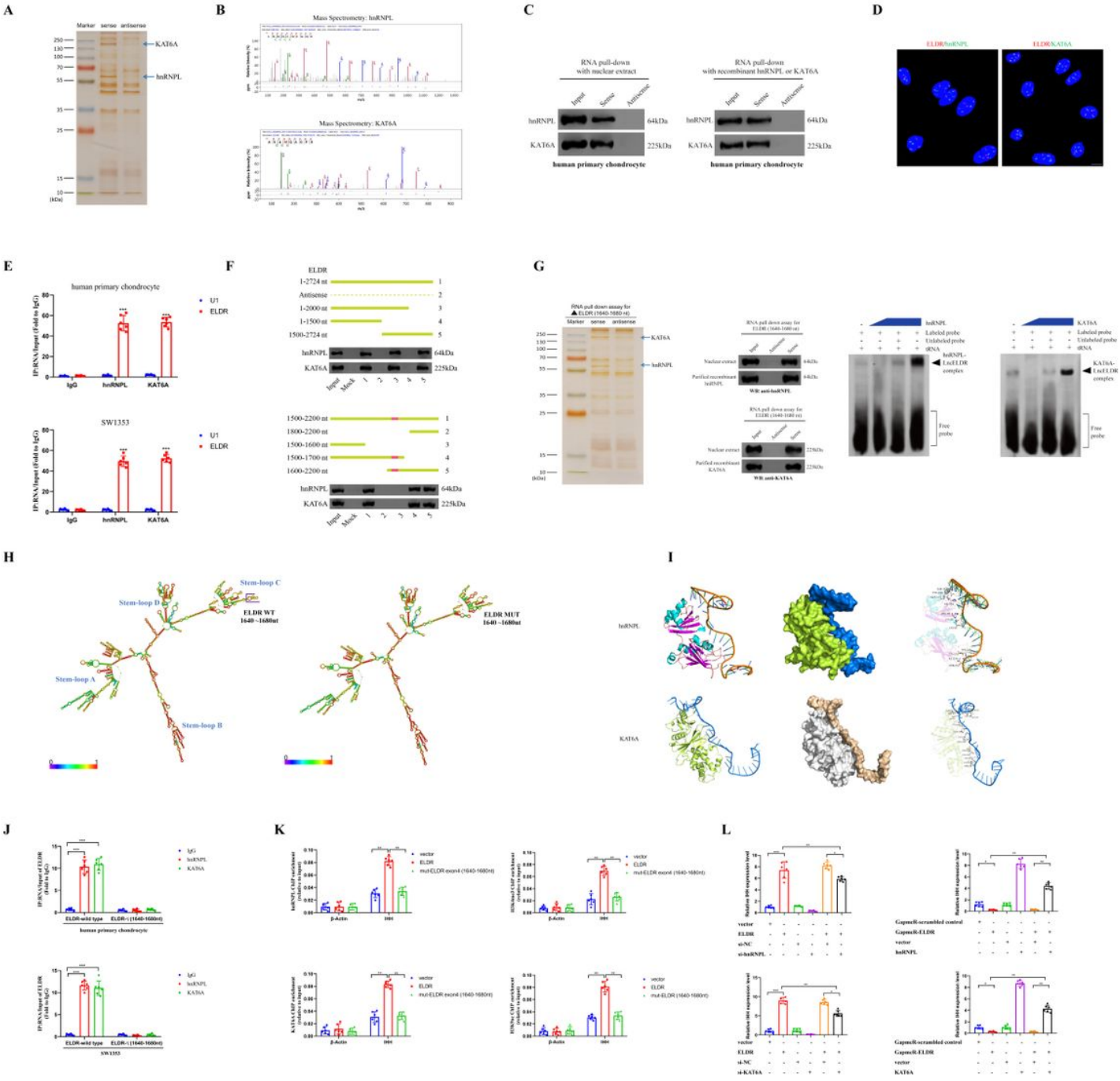

Figure 5

ELDR/hnRNPL/KAT6A promotes H3K4me3 and H3K9ac of IHH promoter

(A-C) Representative image of silver-stained PAGE gels showing separated proteins that were pulled down using biotin-labeled ELDR and arrows indicate hnRNPL and KAT6A (A), further confirmed by mass spectrometry (B) and western blot analysis (C). The cultured human chondrocytes were employed.

(D) RNA in situ hybridization-proximity ligation assay (rISH-PLA) detects the close proximity of a specific RNA with proteins in situ. rISH-PLA confirms the proximity of ELDR to endogenous hnRNPL or KAT6A in the nucleus of cultured human primary chondrocyte. Scale bar, 10μm.

(E) RNA immunoprecipitation (RIP) analysis using the anti-hnRNPL or KAT6A antibody revealed that ELDR interacted with endogenous hnRNPL and KAT6A in cultured human primary chondrocytes and SW1353. U1 was used as the negative control. n=6 biological replicates/group ***P<0.001 by two-tailed unpaired Student's t-test.

(F and G) Serial deletions of ELDR were performed in the RNA pull-down assays to identify the core regions of ELDR for the physical interaction with hnRNPL and KAT6A (F). Silver staining image of proteins pulled down by the 5'-terminus of the truncated ELDR (1640-1680nt). The interaction between the truncated ELDR and hnRNPL or KAT6A was confirmed by RNA pull-down and western blotting with nuclear extract or purified recombinant hnRNPL and KAT6A. hnRNPL and KAT6A proteins and biotin-labeled ELDR (1640-1680nt) probes were incubated for an EMSA assay (G). The cultured human chondrocytes were used.

(H) Four stable stem-loop structure of ELDR was predicted.WT and mutant ELDR were shown.

(I) Interaction model between ELDR (1640-1680nt) and hnRNPL or KAT6A.

(J) RIP analysis performed after site-directed mutagenesis of 1640-1680nt of ELDR in cultured human primary chondrocytes and SW1353. n=6 biological replicates/group; ***P<0.001 by two-tailed unpaired Student's t-test.

(K) ChIP-qPCR analysis of the hnRNPL and KAT6A genomic occupancy and H3K4me3 and H3K9ac in IHH promoter after overexpression or depletion of EDLR in cultured human primary chondrocytes. n=6 biological replicates/group; **P<0.01 by two-tailed unpaired Student's t-test.

(L) Real-time PCR analysis of IHH expression in the hnRNPL or KAT6A knockdown or overexpression or on ELDR-induced IHH expression in cultured human primary chondrocytes. n=6 biological replicates/group; *P<0.05, **P<0.01 and ***P<0.001 by two-tailed t-tests and one-way analyses of variance (ANOVA) followed by Dunnett's tests for multiple comparison.

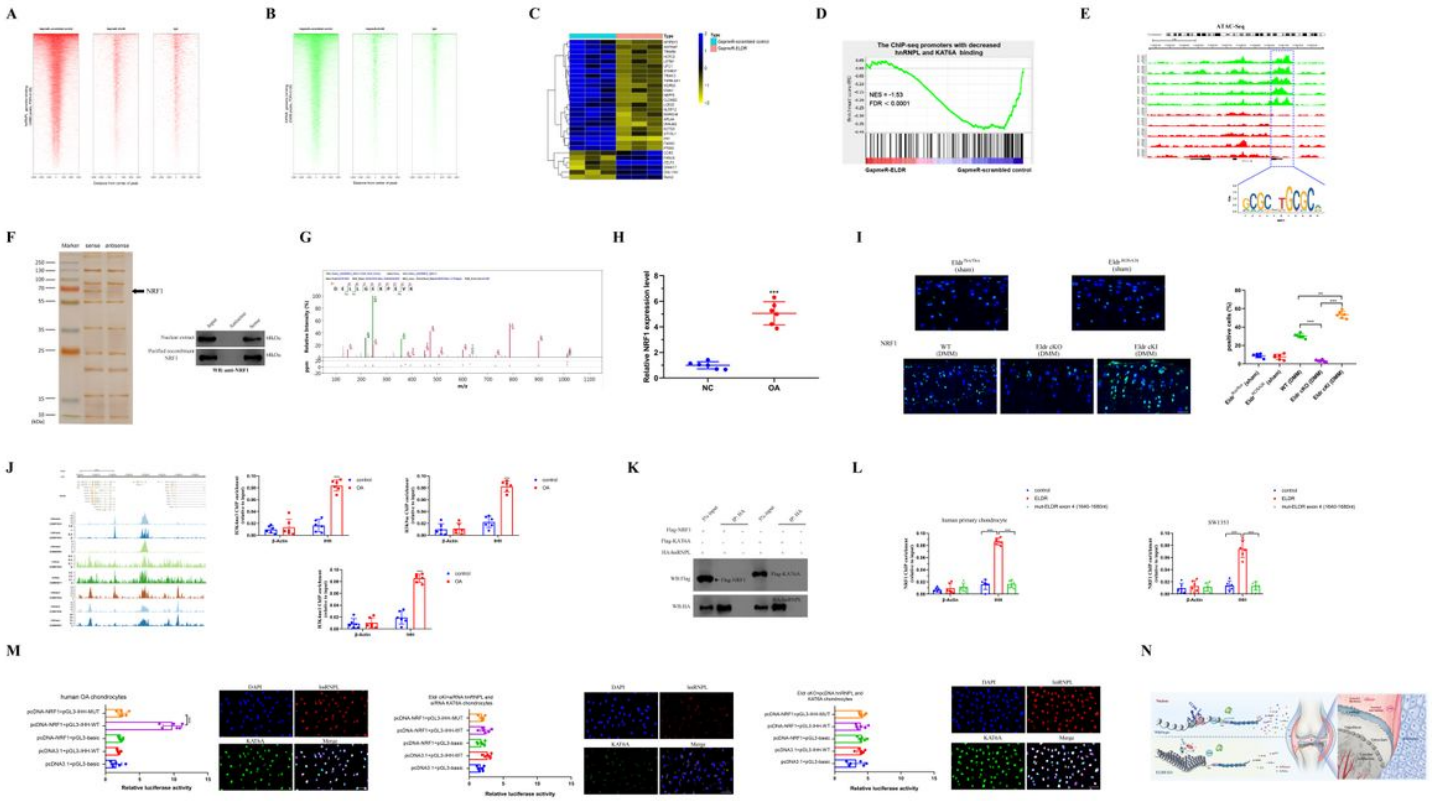

Figure 6

ELDR/hnRNPL/KAT6A creates an open chromatin region in IHH promoter for NRF1 binding

(A and B) Heatmap of hnRNPL (A) and KAT6A (B) global genomic binding at the target sites in chondrocytes after transduction of control and GapmeR-ELDR.

(C and D) Heatmap demonstrating the expression change of hnRNPL/KAT6A co-occupied genes in chondrocytes after transfection of control and GapmeR-ELDR (C) and GSEA data showing the enrichment of ChIP-seq promoter peaks with significant loss of hnRNPL/KAT6A binding for the downregulated genes in chondrocytes after transfection of GapmeR-ELDR (D).

(E-G) ATAC-Seq analysis showing accessible chromatin region in IHH promoter in OA patients and motif enrichment analysis reveals a transcription factor (NRF1) relevant to OA (E), further confirmed by DNA pull down, western blot (F) and mass spectrometry (G)

(H and I) RT-qPCR analysis of NRF1 expression in cultured human primary chondrocytes from OA and controls (H). Immunostaining and quantification of NRF1 in cartilage tissues of the above-mentioned groups (I). n=6 mice/group; Scale bar, 20μm; **P<0.01; ***P<0.001 by two-tailed unpaired Student's t-test (I).

(J) ChIP-Seq analysis demonstrating that the enrichment of H3K4me3, H3K9ac and H3K4me1 in IHH promoter region. The ChIP analysis further confirmed high levels of H3K4me3, H3K9ac and H3K4me1 in

human OA and control chondrocytes in the IHH promoter. n=6 biological replicates/group; ***P<0.001 by two-tailed unpaired Student's t-test.

(K) Co-IP analysis showing the relationships between NRF1 and hnRNPL or KAT6A in chondrocytes.

(L) ChIP-qPCR analysis of the NRF1 genomic occupancy in IHH promoter after overexpression or site-directed mutagenesis of EDLR in human primary chondrocytes and SW1353. n=6 biological replicates/group; ***P<0.001 by two-tailed unpaired Student's t-test.

(M) Using luciferase reporter assays and immunofluorescence, the interaction between NRF1 and IHH promoter was analyzed in different conditions. n=6 biological replicates/group. Scale bar, 20μm. In OA chondrocytes, ELDR, hnRNPL and KAT6A were highly expressed. Thus, ELDR recruits hnRNPL and KAT6A (as confirmed by cell immunofluorescence, i.e., the high co-expression of hnRNPL and KAT6A in the nucleus.) to IHH promoter and promotes its histone modifications, creating an open chromatin status in IHH promoter. As validated by luciferase activity assay, the chondrocytes were co-transfected by pcDNA-NRF1 and pGL3-IHH-WT and the result shows the increase of luciferase activity, indicating the interaction between NRFI and IHH promoter. In ELDR cKI +siRNAhnRNPL and siRNA KAT6A chondrocytes, although high level of ELDR, it can not recruit hnRNPL and KAT6A (as confirmed by cell immunofluorescence) and a closed chromatin status was produced in IHH promoter. As validated by luciferase activity assay, NRF1 can not bind its promoter. In ELDR cKO +pcDNA-hnRNPL and KAT6A chondrocytes, although high level of hnRNPL and KAT6A (as confirmed by cell immunofluorescence), they can not be recruited to the promoter of IHH due to very low level of ELDR. Therefore, the chromatin status of IHH promoter was closed, which precludes NRF1 binding IHH promoter. As validated by luciferase activity assay, NRF1 can not bind its promoter.

(N) Schematic model illustrating the ELDR/hnRNPL/KAT6A complex-mediated transcriptional regulatory model.

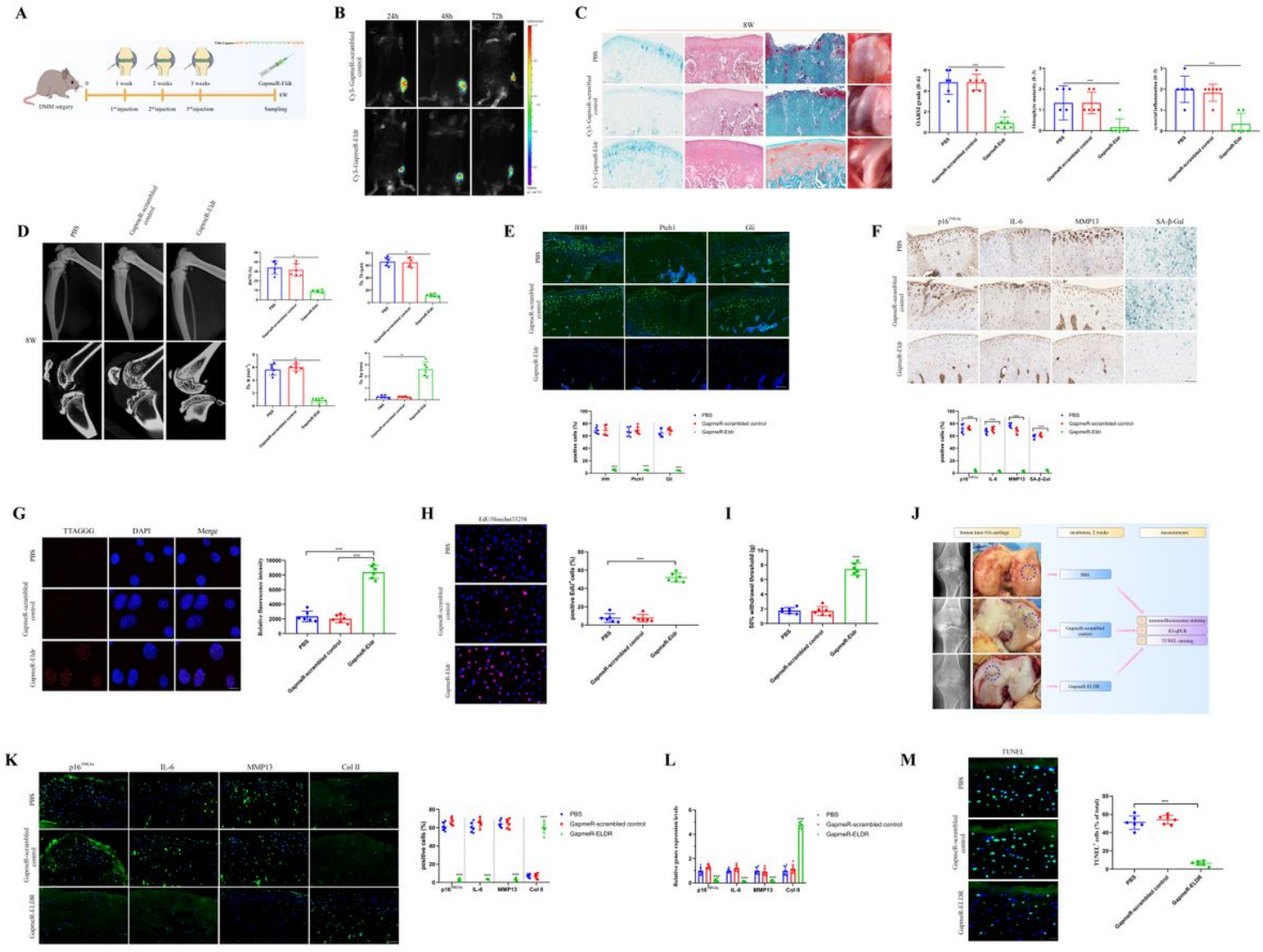

Figure 7

Pharmacological inhibition of ELDR in vivo attenuates chondrocyte senescence and cartilage degradation

(A) Study protocol for examining the effect of GapmeR-Eldr on chondrocyte senescence and cartilage degradation.

(B) In vivo time-dependent fluorescence image in mice at 24, 48 and 72 hours after the administration of Cy3-GapmeR-Eldr or its control.

(C and D) The cartilage degradation evaluated by Alcian blue, HE and Safranin O staining, gross appearance, X- ray and micro-CT in wild type mice subjected to DMM surgery followed by treatment with PBS, GapmeR-scrambled control and GapmeR-Eldr at indicated weeks. Osteoarthritis Research Society International (OARSI), osteophyte formation and synovial inflammation were also quantified respectively.

n=6 mice/group. Scale bar, 100μm. **P<0.01 and ***P<0.001 by one- way ANOVAtest followed by Tukey's post hoc.

(E) Representative images of immunostaining of IHH, Ptch1 and Gli in cartilage from the indicated groups of mice. Scale bar, 100μm. n=6 mice/group.

(F) Representative images of immunohistochemistry of p16INK4a, IL- and MMP13 in cartilage and SA-β-Gal staining in chondrocytes from mice treated with PBS, GapmeR-scrambled control and GapmeR-Eldr, respectively. Scale bar, 50μm. n=6 mice/group.

(G) Representative fluorescence microscopy images of telomere FISH analysis and quantification in chondrocytes from mice undergoing PBS, GapmeR-scrambled control or GapmeR-Eldr treatment, respectively. Scale bar, 10μm. n=6 mice/group.

(H) EdU staining for chondrocytes from mice treated with PBS, GapmeR-scrambled control and GapmeR-Eldr, respectively. Scale bars, 50 μm. n=6 mice/group.

(I) Intra-articular injection of GapmeR-Eldr reduces pain sensitivity induced by chondrocyte senescence and cartilage degradation. The Von Frey test was performed in the 6- month- old mice receiving GapmeR-Eldr injection at the age of 8 weeks. n=6 mice/group. ***P<0.001 by one- way ANOVA test followed by Tukey's post hoc.

(J) Study protocol for ELDR-targeting therapy in clinical OA.

(K-M) Representative images of immunostaining of p16INK4a, IL-6, MMP13 and Col II in human OA cartilage treated with PBS, GapmeR-scrambled control or GapmeR-ELDR, respectively (K). Scale bars, 50 μm. Real-time PCR analysis of p16INK4a, IL-6, MMP13 and Col II (L). ***P<0.001 by one- way ANOVA test followed by Tukey's post hoc. TUNEL staining of human OA cartilage after PBS, GapmeR-scrambled control or GapmeR-ELDR treatment (M). Scale bars, 1 20 μm. n=6 mice/group.

Supplementary Files

This is a list of supplementary files associated with this preprint. Click to download.

- Supplementarydata.pdf